Forward Neutrinos from Charm at Large Hadron Collider

Atri Bhattacharya,[1, *] Felix Kling,[2, †] Ina Sarcevic,[3, 4, ‡] and Anna M. Stasto[5, §]

[1]*Space sciences, Technologies and Astrophysics Research (STAR) Institute,*
Université de Liège, Bât. B5a, 4000 Liège, Belgium
[2]*Deutsches Elektronen-Synchrotron DESY, Notkestr. 85, 22607 Hamburg, Germany*
[3]*Department of Physics, University of Arizona, Tucson, AZ 85721*
[4]*Department of Astronomy and Steward Observatory,*
University of Arizona, Tucson, AZ 85721
[5]*Department of Physics, Penn State University, University Park, PA 16802*

The currently operating FASER experiment and the planned Forward Physics Facility (FPF) will detect a large number of neutrinos produced in proton-proton collisions at the LHC. In addition to neutrinos from pion and kaon decays, a significant contribution is expected from the decay of charmed hadrons, particularly for electron and tau neutrino flavors. In this work, we investigate two QCD formulations for the production of charm quarks in pp collisions: the next-to-leading order collinear factorization and the k_T-factorization approach. We use state of the art fragmentation schemes to obtain hadron cross-sections and validate them against corresponding LHCb data. These calculations are then used to predict the forward neutrino flux from charm hadron decays. We further scrutinize the impact of varying QCD parameters, such as scales, the selection of parton distribution functions, and the modeling of fragmentation, on these predictions. We find that the measurement of forward neutrino flux will serve as a complementary tool to probe QCD dynamics and will offer valuable insights for astroparticle physics.

CONTENTS

* a.bhattacharya@uliege.be

† felix.kling@desy.de

‡ ina@physics.arizona.edu

§ ams52@psu.edu

I. INTRODUCTION

The forward production of charm quarks in high-energy proton-proton collisions at the LHC provides an excellent probe of the strong interactions. In the far forward region, corresponding to pseudorapidity $\eta \gtrsim 7$, which is beyond the coverage of the main LHC detectors, this process is sensitive to parton distribution functions at small momentum fractions $x \sim 10^{-7}$ and at a scale $Q \sim m_c$. In this region of very small-x and small-Q^2, that is not accessible to the direct measurement at HERA [1], deviations from the collinear factorization approach may be expected and novel small-x dynamics can occur, see e.g. Ref. [2]. In particular, the non-linear contributions, which lead to saturation effects of the gluon density are expected to play an important role [3]. Finally, fragmentation functions needed to predict D-meson production are not well known in this regime, as they are usually constrained in e^+e^- collisions, while the hadronic environment of the proton-proton collisions introduces some new dynamical features which may lead to the factorization breaking. Future measurements of forward charm production will therefore provide a unique opportunity to study and test different aspects of QCD in this novel kinematic regime.

The study of forward charm production is also important in the context of large neutrino telescopes, such as IceCube. Here, charmed hadrons can be produced in cosmic ray collisions and their decay constitutes the source of prompt atmospheric neutrinos and hence a background to the extra-galactic neutrino signal [4–6]. There are currently large uncertainties on the associated production rate and flux, underpinned by the lack of input data both at colliders as well as at neutrino telescopes. Indeed, IceCube has not seen evidence of prompt atmospheric neutrinos and only sets an upper limit on the corresponding flux [7]. New input on forward charm production from the LHC will also improve the predictions for prompt atmospheric neutrino production.

The distribution of charmed hadrons at the LHC have been measured in the central region by ATLAS [8], CMS [9, 10] and ALICE [11, 12] and in the forward region by LHCb [13–15]. Together, these measurements cover the pseudorapidities $\eta < 4.5$, while at higher values charm production remains as yet unconstrained. This situation will soon change due to a new set of far forward experiments which will be able to detect and study neutrinos produced at the LHC. Many of these LHC neutrinos originate from the decay of charmed hadrons, and hence a measurement of the neutrino spectrum allows us to indirectly constrain forward charm production. The first two experiments, FASERν [16, 17] covering $\eta > 8.9$ and SND@LHC [18, 19] covering $7.2 < \eta < 8.7$, have started their operation with the beginning of LHC Run 3 in summer 2022. Together, they will detect about ten-thousand neutrino interactions. Larger detectors with the ability to detect about a million neutrino interactions have been proposed in the context of the Forward Physics Facility (FPF) [20–22], which will operate during the HL-LHC era.

In anticipation of first data from the LHC neutrino experiments, it is important to have a dependable modeling of forward charm production and reliable predictions for the resulting neutrino fluxes and their uncertainties. Such estimates of the neutrino flux are needed as input for a variety of planned measurements, for example that of the neutrino interaction cross section. In addition, a comparison of theoretical predictions with the neutrino flux measurements will then allow to constrain QCD parameters, such as the mass of the charm quark, factorization and renormalization scales, parton distributions at small-x, and the fragmentation of the charm into D-mesons. In this paper we address these questions and study charm production at the LHC using two different QCD approaches: the perturbative collinear approach at next-to-leading order (NLO) and the k_T-factorization approach. In particular we constrain our models using available data from LHCb and make predictions for the LHC neutrino experiments. We also investigate the sensitivity of our calculations to the different modeling of the fragmentation of charm quarks into hadrons.

The paper is organized as follows. In Sec. II we review the experimental setup of the LHC

neutrino experiments. We then discuss the modeling of charm production via the perturbative NLO calculation and the k_T-factorization approach in Sec. III. Different approaches to modeling of the fragmentation are discussed in Sec. IV. The main results are presented in Sec. V. Finally in Sec. VI we present our summary and conclusions.

II.   FORWARD NEUTRINO EXPERIMENTS AT THE LHC

The production of flavored hadrons has been extensively studied at all four main LHC experiments. This data provides a crucial input, for example for the modeling of high energy cosmic ray collisions and atmospheric neutrino fluxes. However, the most energetic hadrons are typically produced in the far forward direction, which lies outside of the coverage of the main LHC detectors. These particles are particularly relevant for modeling of cosmic ray collisions, since they carry a large fraction of the air showers energy and are also the source of the most energetic atmospheric neutrinos. While there are some measurements on far forward hadron production using additional LHC detectors, for example on photons and neutrons from LHCf [23, 24], no data exists so far on strange and charm hadrons. Such input would, however, be desirable to address the cosmic ray muon puzzle [25, 26] as well as to improve predictions for prompt atmospheric neutrino flux at neutrino telescopes [4–6]. This situation is changing with the start of the LHC neutrino experiments, which will provide novel constraints on the far forward production of flavored hadrons.

Already in the 1980s it was noticed that the LHC would produce a large number of neutrinos through the decay of hadrons [27]. Indeed, at each collision point the LHC generates an intense and strongly collimated beam of high-energy neutrinos along the beam collision axis. About 480 m downstream from the ATLAS interaction point this neutrino beam passes through the TI12 and TI18 tunnels, which housed the injector during the LEP era but remained empty during the LHC era. These locations provide unique opportunities to access the neutrino beam and study its properties. The first measurement illustrating the potential was performed by the FASER collaboration, which reported the first neutrino interaction candidates using a small pilot detector in 2021 [28]. Following this proof of feasibility, two dedicated detectors have been installed in these locations. Located in TI12 is the FASER experiment [29–31]. While it is mainly designed to search for light long-lived particles predicted by models of new physics [32–36], it also contains a dedicated emulsion neutrino detector called FASERν [16, 17]. This detector is centered on the beam collision axis and covers the pseudorapidity range $\eta > 8.9$. Located in TI18 on the opposite site of ATLAS is SND@LHC [18, 19], which also contains an emulsion target as well as additional electronic components. Unlike FASER, it is positioned slightly off-axis and covers $7.2 < \eta < 8.7$. Both detectors have the ability to distinguish neutrinos of different flavors and measure their energies. With the start of Run 3 of the LHC in summer 2022, both experiments have now started their operation and recently reported the observation of the first collider neutrinos [37, 38]. During LHC Run3, which is expected to last until 2025, the two experiments are expected to detect about ten thousand neutrino interactions with TeV scale energies.

Upgraded detectors to continue the LHC neutrino program are envisioned for the HL-LHC era. These would be located in the FPF [20–22], which is a dedicated cavern to be constructed 620 m downstream of ATLAS with the space to house a suite of experiments. In particular, three dedicated neutrino detectors have been proposed in this context: the emulsion based neutrino detector FASERν2, the electronic neutrino detector AdvSND, and the liquid noble gas based neutrino detector FLArE. Due to a tenfold increase in both target mass and luminosity these detectors have the potential to see more than a million neutrino interactions and study their properties in greater detail.

A first estimate of the neutrino flux has been provided in Ref. [39], taking into account both the prompt flux component from charm decays occurring the interaction point as well as a displaced component from the decay of long-lived light hadrons occurring further downstream from the interaction point. It uses a variety of different MC event generators to model the production of hadrons at the LHC and employs a dedicated fast simulation to model the propagation and decay of long-lived hadrons when passing through the LHC beam pipe and magnetic fields. The results show that a majority of muon neutrinos and electron neutrinos at low energy originate from the displaced decay of light hadrons, while high energy electron neutrinos and tau neutrinos are mainly produced in the prompt decay of charmed hadrons. It was also noted that (i) there are large differences between the MC generator's predictions for the prompt neutrino flux component of about an order of magnitude at high energies, and (ii) most of the generators have not yet been tuned or validated for charm production. More reliable predictions for forward charm production are needed.

Unlike for light mesons, the forward production of charm quarks can be described using pertubative QCD. This provides a different approach to obtain predictions for the LHC neutrino flux, which also offers a deeper connection to the underlying theory of QCD. Several recent studies have presented perturbative calculations for forward charm production at the LHC and derived corresponding predictions for the associated neutrino fluxes. In Ref. [40], the authors employed the collinear factorization approach at NLO, supplemented by additional k_T-smearing and fragmentation functions to account for hadronization effects. Subsequent work by the same authors explored the associated PDF uncertainties [41] and the connection to astroparticle physics [42], also see Refs. [43–45]. In Ref. [46, 47], the authors used the k_T-factorization approach, both in the full and hybrid realization, with fragmentation functions and a recombination model for hadronization. They also investigated the impact of an additional intrinsic charm component on the forward neutrino flux.

In the present analysis, we consider both of these perturbative QCD approaches. Specifically, we systematically analyze the influence of varying QCD parameters, such as scales, the choice of parton distribution functions, and the modeling of fragmentation, on the predictions for the charm production at LHCb and forward neutrino fluxes at FASER. In the following sections, we provide detailed descriptions of the forward charm production modeling employing both approaches.

III. CHARM QUARK PRODUCTION IN HADRONIC COLLISIONS

The standard routine for calculating the charmed hadron production cross section σ_H is to fold the hadronic charm quark cross section σ_c with a fragmentation function $F_{c \to H}$

$$\sigma_H \sim \sigma_c \otimes F_{c \to H} . \tag{1}$$

In this section, we first focus on the perturbative calculation of charm quark production in hadronic collisions. In particular, we will describe and utilize two QCD approaches to calculate charm quark production: the NLO collinear factorization formalism and the k_T-factorization formalism. A detailed discussion of fragmentation into hadrons will then be provided in Sec. IV.

The production of charm in hadronic collisions is dominated by the gluon-gluon scattering. In this process, gluons from two colliding hadrons fuse and produce a charm quark-antiquark pair which subsequently fragments into the hadrons. The generic diagram for gluon-gluon fusion process in hadronic collision is illustrated in the left panel Fig. 1, where the cross section can be factorized into two gluon distribution functions, f_1 and f_2, and the perturbatively calculable partonic cross section $\hat{\sigma}$. This is the framework at the root of collinear factorization approach.
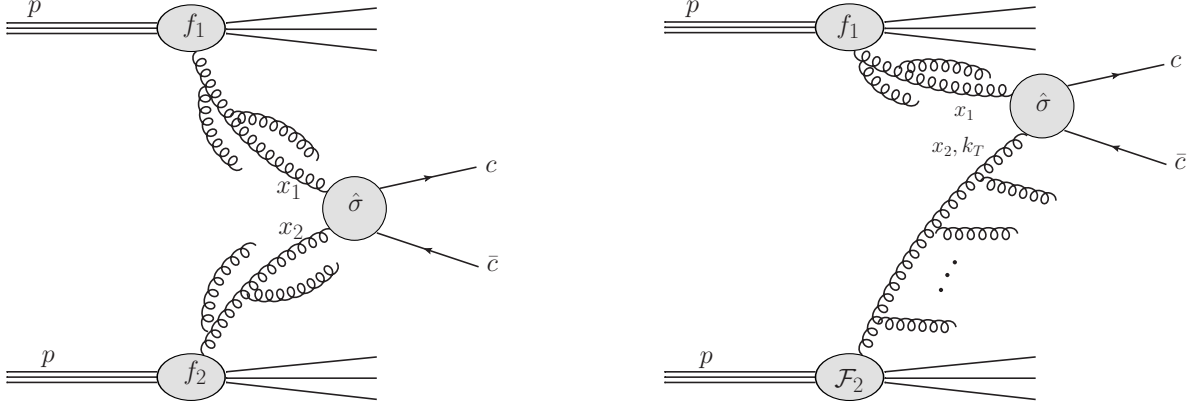
FIG. 1. Left: gluon-gluon fusion process for charm production in hadron-hadron collisions in the collinear factorization approach. f_1, f_2 are the integrated gluon distribution functions which depend on the longitudinal momentum fractions x_1, x_2 and the hard scale of the partonic sub-process. Right: the same process, illustrated for the case of forward production in the k_T-factorization. The gluon x_1 is treated on-shell, and the gluon x_2 is off-shell with transverse momentum k_T. $\hat{\sigma}$ is the partonic cross section which is on-shell (left panel) and takes into account off-shellness of one gluon (right panel).

In the forward region, this process probes the kinematics where the two incoming partons have very different longitudinal momenta. The longitudinal momentum of the forward charm quark at high energy is approximately equal to $x_F \simeq E_c/E_p$ where E_p is the energy of the incident proton and E_c is the energy of the charm quark. Since we are interested in TeV-energy neutrinos from TeV-energy charm decay, the corresponding forward charm production kinematics probes values of x_F of order 0.1 or higher. This in turn means that the longitudinal momentum fraction of one of the gluons is large, $x_1 \sim x_F$, and the other one is very small. To be precise the longitudinal momentum fraction $x_2 \simeq m_{c\bar{c}}^2/(x_F s)$, where $m_{c\bar{c}}$ is the invariant mass of the produced charm-quark pair and $\sqrt{s}$ is the center of mass energy of the hadronic collision. This means that for high energies the forward production is particularly sensitive to the gluon density at very low values of $x_2 \gtrsim 10^{-7}$, which is not constrained very well in this region. Thus the forward production offers unique possibilities for tests of novel QCD dynamics in the region of small-x.

A. Collinear Factorization at NLO

The double differential NLO cross-section for charm pair production is given by the expression

$$\frac{d^2\sigma_{pp}}{dydp_T^2}(s, m_c^2) = \sum_{i,j=q,\bar{q},g} \int dx_1\, dx_2\, f_i(x_1, \mu_F^2)\, f_j(x_2, \mu_F^2)\, \frac{d^2\widehat{\sigma}_{ij}}{dydp_T^2}(\hat{s}, m_c^2, \mu_F^2, M_R^2)\,, \qquad (2)$$

where m_c is the charm mass, $\sqrt{\hat{s}} = \sqrt{x_1 x_2 s}$ is the partonic CM energy, μ_F and μ_R are the factorization and renormalization scales respectively, and $f_{i,j}$ represent the quark and gluon parton distribution functions (PDFs) as appropriate. As noted previously, we compute the cross-section to the next-to-leading order in perturbation theory.

The double differential cross-sections for charm quark production are calculated using the FONLL code [48, 49], which provides an interface to LHAPDF [50, 51], thus allowing one to use a variety of up-to-date PDFs. We choose to use the central CT14nlo PDF set [52] from the LHAPDF database as a representative set for our analysis. While there are more recent PDF sets available in the

literature, including those that have been fit to 13 TeV LHCb data and consequently have reduced uncertainties in their predictions at low-x [53, 54], we find that uncertainties in the cross-section from scale variation dwarf those from using different PDFs. Instead, our choice of the central `CT14nlo` PDF allows us to maintain compatibility with results obtained in Ref. [4], while also using $m_c = 1.3$ GeV, consistent with the PDG best-fit.

To obtain best-fits to current charm data, we choose to vary the factorization scale μ_F and renormalization scale μ_R while keeping the charm mass fixed. Assuming the scales vary proportionally to the charm transverse mass, $m_T = (m_c^2 + p_T^2)^{1/2}$, it has been the norm to vary these parameters independently within a range from $(0.5$–$2.0) \propto m_T$. However, when restricting ourselves to this narrow range, we find that at high energies $\sqrt{s} \geqslant 7$ TeV fits to data become progressively worse with increasing rapidities. Furthermore, determining uncertainties around the best-fit scales also requires one to extend the search beyond this range. Therefore, we allow these parameters to vary independently over a broader range $\in [0.5, 8.0]$ unencumbered by theoretical preferences, allowing the best-fit parameters to be instead determined by fitting to data. We also determine the parameters defining a 1σ uncertainty band around the best-fit cross-section.

To determine the correct global best-fits for these scales, one ought to use all the available data for charm production in pp collisions and determine the cross-section that gives the least value of $\Delta\chi^2$. However, for our specific study where predictions for the forward neutrino flux are the end goal, we need cross-sections that accurately describe the data at high energies $\sqrt{s} \sim 13$ TeV and high rapidities. The highest rapidity $d^2\sigma/dydp_T$ data at 13 TeV come from charmed meson cross-sections observed at LHCb [14]. These include cross-sections for $D^0, D^\pm,$ and D_s at rapidities between $2 \leqslant y \leqslant 4.5$ binned by 0.5, i.e. five bins in y for each meson. We focus on this subset of collider data to determine the scales, μ_R and μ_F, that best describes it.

To compare our theoretical cross-sections against charmed meson cross-sections from LHCb, we first compute the double differential cross-section $d^2\sigma_{c\bar{c}}/dydp_T$ for bare $c\bar{c}$ pair production using specific values for the fragmentation and renormalization scales. We then assume a specific fragmentation scheme, without any additional free parameters, to hadronize the charm quarks into hadrons. The resulting differential cross-section distribution at this stage may now be compared against corresponding LHCb data for a measure of its goodness of fit, which we achieve by means of a simple χ^2 analysis. Since accurately forecasting high rapidity cross-sections is critical towards obtaining predictions for forward experiments like FASER, it becomes important to ensure that the goodness of fit analysis is not skewed by the availability of significantly more data at LHCb's lower rapidities $2 \leqslant y \leqslant 3$ rather at, say, $y \geqslant 4$. We therefore use a χ^2 measure that is normalised to the number of p_T bins with cross-section measurements for each rapidity bin in the LHCb data, ensuring that each bin carries equal weight towards the measure.

Repeating this procedure for multiple (μ_R, μ_F) values, we generate a range of cross-sections and, for a given fragmentation scheme, we ascertain the best-fit value of these parameters as the one that minimises the χ^2/d.o.f. Likewise, we also obtain the parameters corresponding to a 1σ region of variation around the best-fit cross-section. The end result of this exercise is that we obtain a set of best-fit (μ_R, μ_F) for each choice of fragmentation scheme.

B. k_T-factorization

In the forward regime, one should apply a framework which incorporates resummation of the large logarithms $\alpha_s \ln 1/x$. This is accomplished through the k_T-factorization formalism [55–57]. The k_T-factorization formalism involves off-shell matrix-elements for partonic scattering and unin-

tegrated gluon distribution[1] functions $\mathcal{F}(x, \mathbf{k}_T)$ which depend on the transverse momentum vector $\mathbf{k}_T$ of the off-shell gluons. The unintegrated gluon distribution functions encode more detailed information about the dynamics of the partons, and can be especially important in providing information about the details of the kinematics of the event. The k_T-factorization approach in hadroproduction of heavy quarks has been considered in Refs. [55–57] where the off-shell matrix element for heavy quark production have been derived. The expression for the cross section in the k_T-factorization formalism has the following form, see e.g. [55]

$$\sigma_{pp}(s, m_c^2) = \int dx_1 \, dx_2 \, \frac{d^2\mathbf{k}_{1T}}{\pi} \frac{d^2\mathbf{k}_{2T}}{\pi} \mathcal{F}(x_1, \mathbf{k}_{1T}) \, \mathcal{F}(x_2, \mathbf{k}_{2T}) \, \widehat{\sigma}^{\mathrm{off}}(\hat{s}, \mathbf{k}_{1T}, \mathbf{k}_{2T}, m_c) \,. \tag{3}$$

For the specific case of forward charm production considered here, due to the fact the the kinematics is very asymmetric and one gluon has large longitudinal momentum fraction x_1 it is appropriate to use an approach in which this gluon is treated on-shell and satisfies the DGLAP evolution. Therefore the formula Eq. (3) in this limit becomes

$$\sigma_{pp}(s, m_c^2) = \int dx_1 \, dx_2 \, \frac{d^2\mathbf{k}_T}{\pi} \, f(x_1, \mu^2) \, \mathcal{F}(x_2, \mathbf{k}_T) \, \widehat{\sigma}^{\mathrm{on-off}}(\hat{s}, \mathbf{k}_T, m_c) \,, \tag{4}$$

where $\widehat{\sigma}^{\mathrm{on-off}}$ can be obtained from $\widehat{\sigma}^{\mathrm{off}}$ by setting one gluon on-shell, see Ref. [55]. This is illustrated in the right panel of Fig. 1. The gluon with large longitudinal momentum fraction x_1 is indicated together with schematically drawn collinear cascade originating from one proton. On the other hand, the gluon with very small x_2 has transverse momentum k_T and it is produced as a result of a very long cascade of emissions from the other proton. These emissions are not collinear, hence their transverse momenta are not ordered. Therefore such cascade leads to the diffusion in the transverse momentum distribution. This approach was used in Ref. [2] with the large x_1 gluon in the DGLAP collinear regime, which is on-shell and the small x_2 gluon off-shell, with appropriate approximation of the matrix element.

In this work we are interested in the differential distributions in rapidity, which can be obtained by generalizing collinear formula Eq. (2) to include the transverse momentum dependence. Since we are using expressions from [55], which are formally lowest order, the differential cross section can be taken as

$$\frac{d\sigma}{dy_3 dy_4 d^2\mathbf{p}_{3T} d^2\mathbf{p}_{4T}} = \int \frac{d^2\mathbf{k}_T}{\pi} \frac{\delta^{(2)}(\mathbf{k}_T - \mathbf{p}_{3T} - \mathbf{p}_{4T})}{16\pi^2(x_1 x_2 s)^2} x_1 g(x_1, \mu^2) \mathcal{F}(x_2, \mathbf{k}_T) \overline{\sum} |\mathcal{M}_{gg^* \to c\bar{c}}^{\mathrm{on-offshell}}|^2 \,, \tag{5}$$

with momentum fractions $x_1 = \frac{m_{3T}}{\sqrt{s}} \exp(y_3) + \frac{m_{4T}}{\sqrt{s}} \exp(y_4)$ and $x_2 = \frac{m_{3T}}{\sqrt{s}} \exp(-y_3) + \frac{m_{4T}}{\sqrt{s}} \exp(-y_4)$ as well as the transverse masses $m_{3,4T}^2 = p_{3,4T}^2 + m_c^2$ of the quark and antiquark (see also [46]).

The unintegrated gluon distribution functions within the high-energy formalism need to be computed from the appropriate evolution equations which incorporate the small-x dynamics. The unintegrated parton densities within the high energy formalism are usually computed from the Balitsky-Fadin-Kuraev-Lipatov (BFKL) equation which resums the powers of $\alpha_s \ln 1/x$ [61, 62]. It has been computed at leading logarithmic (LL) and next-to-leading logarithmic order (NLL) in QCD. For the phenomenological applications it needs to be supplemented by the additional corrections which take into account higher orders in the form of kinematical constraints and the constraints from matching to the DGLAP evolution [63]. In addition, in the limit of high energies,

---

[1] In the context of the small-x physics one traditionally used the nomenclature of unintegrated parton distribution functions. There is another formalism, see e.g. [58], in which the corresponding parton density functions are also transverse momentum dependent, they are usually referred as TMDs. Relations between the two formalisms have been extensively studied recently, see e.g. [59],[60].

or very small-x, other corrections are expected to occur, which are related to the parton saturation phenomenon [3]. In this regime, the gluon densities are so large that recombination effects need to be taken into account which are expected to slow down the growth of the gluon densities and as a result restore the unitarity of the cross sections, which otherwise might be violated. These corrections lead to the appearance of the non-linear terms in the small-x evolution equations. The non-linear evolution leads to the taming of the gluon distribution in the region of very small-x and moderate to small values of scales k_T. To be specific, these evolution equations generate the x-dependent saturation scale $Q_s^2(x)$. Whenever the relevant scale of the process, say the k_T of the gluon, is smaller than $Q_s^2(x)$ non-linear terms are very important, while for $k_T^2 > Q_s^2(x)$ they can be neglected and the non-linear evolution equations give results which coincide with thus obtained form the linear evolution.

The effective theory for high density at small-x is the Color Glass Condensate [64–69], with the corresponding JIMWLK evolution equations. In the multicolor limit the hierarchy of JIMWLK equations reduces to the Balitsky-Kovchegov equation [70, 71], the latter being the BFKL equation supplemented with the nonlinear term in the gluon density.

The small-x unintegrated gluon density for the present paper was taken from Ref. [72] as well as from Ref. [73]. The gluon in Ref. [72] which was based on the unified BFKL+DGLAP evolution supplemented with small-x resummation [74]. Two sets of gluon distributions were used: based on linear evolution as well as non-linear evolution cast in the momentum space [75, 76]. The latter one includes the non-linear term in density which is responsible for the saturation effects. Both sets of distributions were fitted to the data on F_2 structure function at HERA. The non-linear term is important for low-x and low values of transverse momenta and leads to taming of the gluon distribution and therefore the resulting observable cross section. We also used the gluon extracted from more recent fit in Ref. [73] to HERA data, which was based on the full resummation [63, 77] including the BFKL at NLO.

IV. CHARM FRAGMENTATION

In the previous section we have discussed the perturbative aspects of charm production. We now turn to question of fragmentation of charm quarks into charm hadrons, which is a non-perturbative process and requires a separate treatment.

Many studies of charm production at the LHC make use of the factorization theorem to separate the charm production and fragmentation process. The latter is then modelled via fragmentation functions that have been extracted from lepton collider data. Here one uses the fact that charm quarks in electron-positron annihilation are produced with a known momentum, for example with $p_c = m_Z/2$ at LEP. One can then measure the flavor and momentum of charmed hadrons p_H to constrain the fragmentation process. This is typically parameterized in terms of fragmentation fractions f_H, describing the probability of a charm quark to form a specific charm hadron H, and a fragmentation function $D_H(z)$, describing the distribution of fractional energy inherited by the hadrons $z = p_H/p_c$. In this work, we use the fragmentation fractions $f_{D^+} = 0.244$, $f_{D^0} = 0.606$, $f_{D_s^+} = 0.081$ and $f_{\Lambda_c^+} = 0.061$ as obtained in Ref. [78] and the *Peterson* fragmentation function [79]. It has the form $D_H(z) \sim z^{-1}[1 - 1/z - \epsilon/(1-z)]^{-2}$ where we choose $\epsilon = 0.035$ following Ref. [80]. Note that the same fragmentation function is used for all charmed hadrons. Mainly for illustration, we will also consider the trivial case with *no fragmentation* beyond fragmentation fractions. This means that quark and hadron momenta are identical, implying $D_H(z) = \delta(z - 1)$.

Although the above-mentioned fragmentation functions approach has been successfully applied to measurements of charm production in the central and high-p_T region of the LHC, it faces

additional challenges in the forward and low-p_T regime. There are a variety of hadron collision measurements that contradict the predictions obtained using fragmentation function; see Sec. 6.2.2 of Ref. [22] for a pedagogical overview. In the following, we summarize four important observations that are particularly relevant for the modeling of forward charm production:

- The first observation concerns the *production asymmetry* of charmed mesons and their anti-particles. While the fragmentation function approach predicts equal production rates of charmed hadrons and their anti-particles, an excess of D^- compared to D^+ has been observed at high x_F in π^--nucleus fixed target collisions recorded by WA82 [81], E769 [82] and E791 [83]. Such production asymmetries in the forward direction are typically explained by charm hadronization involving the beam remnants [84]. In the case of π^--nucleus collisions, the $\bar{c}$ can hadronize with the valence d from the pion and form an energetic D^- meson. In contrast the formation of a D^+ requires a c and $\bar{d}$. Since the $\bar{d}$ cannot be a valence quark, but either a sea-quark or produced otherwise, the D^+ mesons are expected to be less energetic. This effectively induces a production asymmetry at high x_F.

- The second observation regards the *energy spectra*. Using the same data from pion fixed target experiments, it has been found that the momentum spectrum charm of hadrons are about as hard as or even harder than the charm quark spectra obtain from perturbation theory [81–83]. This contradicts the fragmentation functions approach, which predict the hadrons to be softer than the charm quarks. In contrast, the above-mentioned mechanism of hadronization with other light quarks in the event, especially valence quarks from the beam remnant, would naturally allow the hadrons to be more energetic than the charm quarks and explain this observation.

- The third observation relates to the *baryon to meson production ratios*. Recently, ALICE has measured the ratio between the Λ_c baryon and D^0 meson production rates in the central region and found that this ratio increases from about 10% at high transverse momentum to about 50% at low transverse momentum [85–87]. A similar enhancement was also seen by CMS [88]. This disagrees with the expectation from fragmentation functions, which predict a roughly constant Λ_c to D^0 ratio of around 10%.

- A fourth observation regards the *multiplicity dependence*. The ALICE experiment has measured the open D-meson production rate in proton-proton collisions as a function of the charged multiplicity. They found that the D-meson yields grows faster than linear with increasing multiplicity and that this growth is even steeper at large transverse momenta [89, 90]. This dependence of the charm hadron distribution on the hadronic environment is not captured in the fragmentation function approach.

The four observations above illustrate that fragmentation functions extracted from lepton colliders are not sufficient to describe charm production at hadron colliders.

One way to address this problem is to use more sophisticated models of fragmentation which are typically implemented in MC generators. Here, we will take advantage of these efforts and use `Pythia 8` [91, 92] to model hadronization. `Pythia` uses the Lund string model [93, 94] in which colored objects are connected by a color string containing the field lines of the strong force. This model can intuitively explain two of the above observations: a charm quark connected to a beam remnant valence quark will be pulled forward, and hence gain energy, or even hadronize together with the valence quark, leading to a production asymmetry. By default, `Pythia` uses the *Monash* tune [95]. While broadly used to describe phenomena at the LHC, we note that it is not able to properly describe the baryon enhancement observed at ALICE. This problem is addressed by a

newer *QCD-inspired color reconnection* scheme introduced in Ref. [96]. It allows for different string topologies, such as junctions of three strings, which leads to a higher baryon production rates in high-multiplicity regions. It has been also recently suggested [97], using modeling with `Pythia`, that this QCD-inspired color reconnection mechanism might be essential for the proper description of the J/ψ production at the LHC. In this work, we use the `mode 2` configuration introduced in Ref. [96].

In the fragmentation function approach, we explicitly convoluted the charm quark distribution $d^2\sigma_c/(dp_{T,c}dy_c)$ with a function function $D_H(z)$ to obtain the hadron level distribution $d^2\sigma_H/(dp_{T,H}dy_H)$. The hadronization procedure in MC generators is more complex and cannot easily be described by a simple function. We therefore follow a different approach in this case and use a re-weighting procedure which is inspired by Ref. [98]. The charm production process of `Pythia` provides a sample of events, where each event is characterized by the parton momentum $\vec{p}_c$, the hadron momentum $\vec{p}_H$, a hadron ID and an event weight w. The events in the sample implicitly follow a distribution $d^2\sigma_c^{P8}/(dp_{T,c}dy_c)$ for the charm quarks and $d^2\sigma_H^{P8}/(dp_{T,H}dy_H)$ for the charm hadrons. In the re-weighting procedure, we can now adjust the weights

$$w \to w \times \frac{d^2\sigma_c/(dp_{T,c}dy_c)}{d^2\sigma_c^{P8}/(dp_{T,c}dy_c)} \ . \tag{6}$$

By construction, the events will then follow a $d^2\sigma_c/(dp_{T,c}dy_c)$ at quark level. The hadrons follow the desired distribution $d^2\sigma_H/(dp_{T,H}dy_H)$ which we can extract from the event sample.

V. RESULTS

In this section, we present and discuss the results of our different charm production models. We start this by systematically varying the modeling. For each considered setup, we shall show comparisons of our predictions to the double differential cross section of D^0 meson measured at 13 TeV by LHCb as well as the expected neutrino event rates at FASERν. To determine the neutrino flux, we follow the same approach as Ref. [39]. Initially, the charm hadrons are decayed in their rest frame according to the decay branching fractions and energy distributions obtained with `Pythia`. Subsequently, the resulting neutrinos are boosted into the laboratory frame and recorded if they pass through the detector's cross-sectional area. To obtain the anticipated number of neutrino interactions, we convolute the neutrino flux with the interaction cross-sections obtained by `GENIE` [99].

In the following, we will present results for collinear factorization in Sec. V A and k_T-factorization in Sec. V B. We will compare both approaches and show additional distributions in Sec. V C.

A. Collinear Factorization at NLO

We first consider the calculation using the NLO collinear factorization. As described in Sec. III A, we obtain multiple best-fit cross-sections corresponding to different fragmentation schemes. We find that a variation of the scale parameters (μ_F, μ_R) mainly influences the normalization of the cross-section predictions, while the shape of the p_T distribution remains largely unchanged. In contrast, the latter is more significantly affected by the choice of the fragmentation scheme.

We show a comparison of these results to the LHCb data in the left panel of Fig. 2 for three different modeling approaches for fragmentation. The green dotted line shows the best fit prediction obtained using a constant fragmentation factor. The best-fit cross-section in this case is obtained
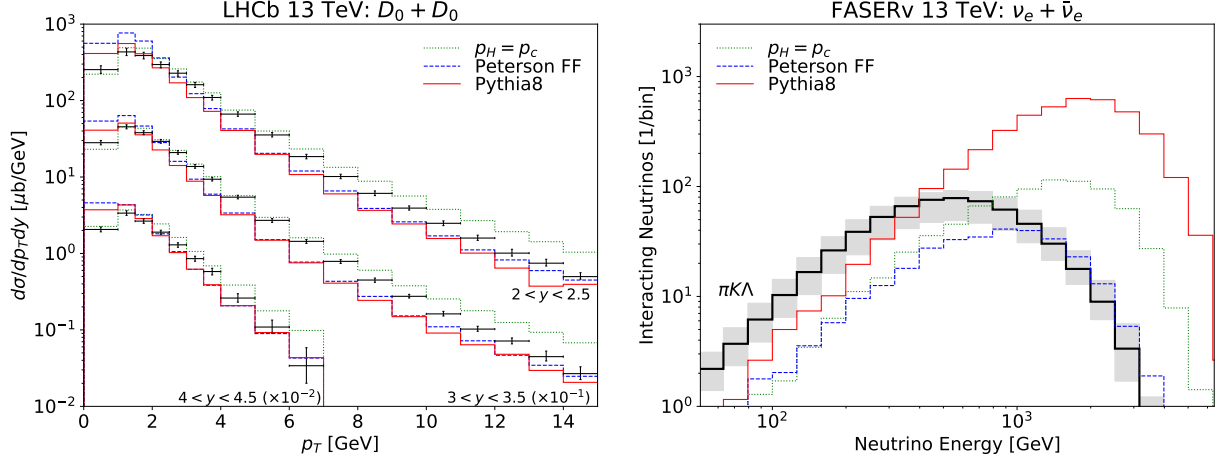
FIG. 2. **Modeling of Fragmentation:** Predictions obtained using collinear factorization at NLO using the `CT14nlo` parton distribution functions. We show three different modeling approaches for fragmentation using only fragmentation fractions (green dotted), using the Peterson fragmentation function (blue dashed), and using `Pythia` with the QCD-inspired color reconnection scheme (red solid). For each approach, the scales were obtained using a fit to LHCb open charm data resulting in $(\mu_F, \mu_R) = (2.1, 1.6) \, m_T$ (no fragmentation function), $(\mu_F, \mu_R) = (3.75, 1.75) \, m_T$ (Peterson fragmentation function) and $(\mu_F, \mu_R) = (2.25, 1.5) \, m_T$ (`Pythia`). In the left panel, we compare these predictions with measurements of the double differential neutral D-meson production rate obtained by LHCb at 13 TeV. We present results for three different rapidity regions, where the results at higher rapidity were scaled. In the right panel, we show the resulting number of electron neutrinos from charm hadrons decay that interact with the FASERν detector as a function of the neutrino energy. For context, we also display in black the event rate resulting from neutrinos from light hadron decays as obtained in Ref. [39]. See the main text for a detailed discussion.

for $(\mu_F, \mu_R) = (2.1, 1.6) \, m_T$ consistent with results from [4]. However, we find that the p_T shapes of the corresponding double differential cross-sections are inconsistent with LHCb data, consistently overestimating at high p_T. With change of scales primarily affecting cross-section normalizations, and not the shape, there is no way to improve the fit within the realm of our analysis when using constant factors for fragmentation. Thus, this demonstrates the importance of including more realistic fragmentation schemes. The blue dashed lines show the best fit results using the Peterson fragmentation function, obtained for $(\mu_F, \mu_R) = (3.75, 1.75) \, m_T$. These agree reasonably well with LHCb data for all rapidity regions, while still overestimating the data at low p_T somewhat. Finally, best-fit results obtained using `Pythia` for fragmentation are shown as red solid lines. These correspond to $(\mu_F, \mu_R) = (2.25, 1.5) \, m_T$. We observe that this setup produces similar results to those using the Peterson fragmentation function in the regime accessible to LHCb, with slight differences mainly at low $p_T < 2$ GeV.

We proceed to evaluate the electron neutrino flux from charm hadron decay at FASERν from these simulations. The results are shown in the right panel of Fig. 2. With Peterson's fragmentation, the obtained flux has lower rates and peaks at lower energies compared to the scenario without any fragmentation. This outcome is expected since in the fragmentation function approach, the charm hadron is always less energetic than the charm quark. In contrast, using `Pythia` for fragmentation increases the neutrino flux and shifts it to higher energies compared to the scenario without any fragmentation. As discussed in Sec. IV, this outcome is consistent with observations at beam dump experiments, where hadronization with beam remnants plays a role. We emphasize that despite both fragmentation choices providing similarly good descriptions of the LHCb data, they lead to a significant difference in neutrino event rates at FASERν, differing by about one order of
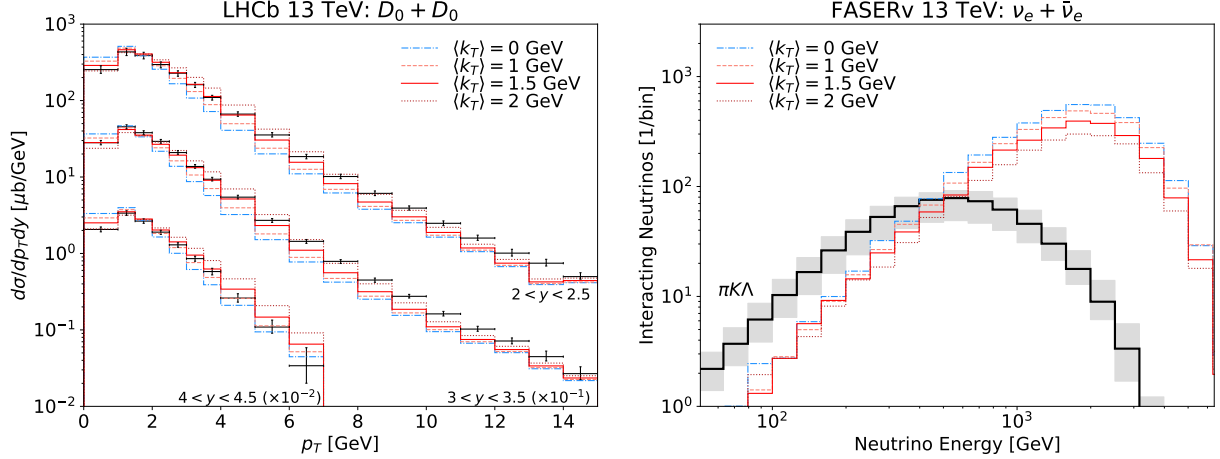
FIG. 3. **Smearing of k_T in Collinear Factorization:** Predictions using collinear factorization at NLO including k_T smearing for different values of $\langle k_T \rangle$. All predictions use fixed scales $(\mu_F, \mu_R) = (1.75, 1.25)\, m_T$, the `CT14nlo` parton distribution function and `Pythia` with the QCD-inspired color reconnection scheme to model fragmentation. See the main text for a detailed discussion.

magnitude. This highlights the importance of properly modeling fragmentation for forward charm and, consequently, neutrino flux predictions for FASERν and other LHC neutrino experiments. For comparison, we also show the event rate from light hadron decays in black, as obtained in Ref. [39], using various generators. The solid line represents the central prediction, while the shaded band shows the range of predictions from different generators. This line is meant to provide optical guidance and to illustrate regions where light and charm hadron decay contributions dominate the electron neutrino flux.

While our prediction already agrees reasonably with the LHCb data, we observe an underestimation of events at intermediate $p_T \sim 8$ GeV and a mild overestimation at $p_T \sim 1$ GeV when compared to experimental measurements. As pointed out in Ref. [40], including an additional k_T smearing, which aims to capture both an intrinsic transverse momentum of the initial state partons as well as some soft gluon emission effects, can help improve the agreement with data. The authors achieve this by introducing a Gaussian smearing with width $\langle k_T \rangle$ of the transverse momentum of the charm, while keeping its rapidity constant. However, we note that this approach does not conserve energy and can lead to charm quarks that are more energetic than the proton beam. Indeed, this leads to an unphysical order of magnitude increase of the neutrino event rate at high energies. To address this issue, we modify the smearing such that the z component of charm quark momentum is kept constant and the rapidity is allowed to change.

In Fig. 3, we present our results when applying the smearing with different values of $\langle k_T \rangle$ to our central prediction. In this case, when using $\langle k_T \rangle = 1.5$ GeV, our fitting routine leads to a best-fit $(\mu_F, \mu_R) = (1.75, 1.25)\, m_T$. As shown in the left panel, the shape of the transverse momentum distributions in the LHCb range changes: events are shifted from the lowest p_T bins towards intermediate p_T bins. This effect becomes stronger with increasing $\langle k_T \rangle$, and by scanning fits made using different fixed values for $\langle k_T \rangle = 0, 0.5, 1.0, 1.5, 2.0 \ldots$, we find that the best agreement with data is obtained for $\langle k_T \rangle = 1.5$ GeV. This value is consistent with Ref. [42], which uses $\langle k_T \rangle = 1.2$ GeV, as well as with the default transverse momentum for hard interactions used within `Pythia`, which is 1.8 GeV. The corresponding neutrino fluxes are not highly sensitive to the choice of $\langle k_T \rangle$, as illustrated in the right panel.

Up to now, we've only shown our central prediction, which uses scale choices $(\mu_F, \mu_R) =$
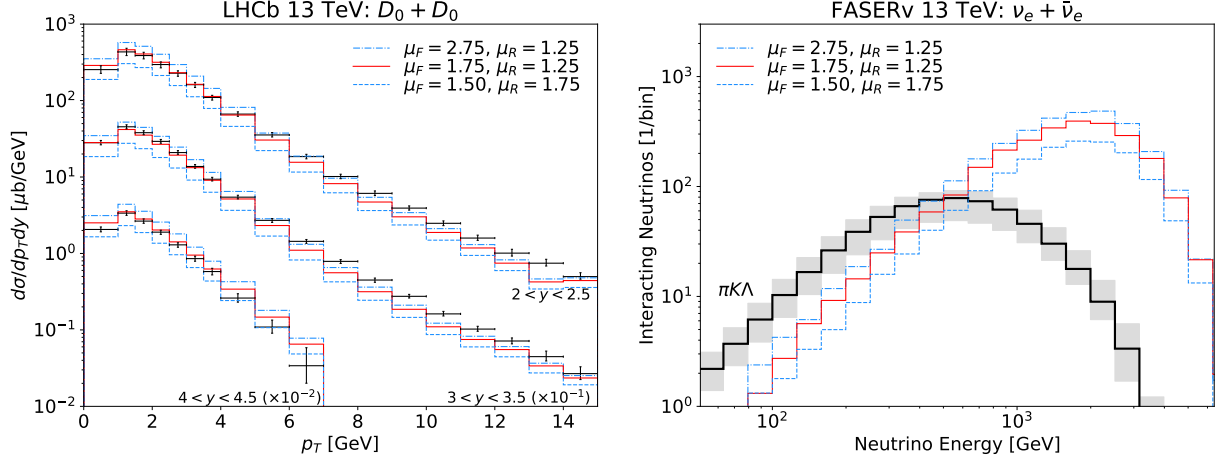
FIG. 4. **Scale Variation in Collinear Factorization:** Predictions using collinear factorization at NLO with different choices of scales μ_F and μ_R. All prediction use the `CT14nlo` parton distribution function, k_T smearing with $\langle k_T \rangle = 1.5$ GeV and `Pythia` with the QCD-inspired color reconnection scheme to model fragmentation. See the main text for a detailed discussion.

$(1.75, 1.25)$ m_T that were obtained by fitting the data with $\langle k_T \rangle = 1.5$ GeV. As described in Sec. III A, the same fit also allows to define scale uncertainties in a data driven way. To illustrate this, we present in Fig. 4 our results for two additional scale choices, which provide an error band that encompasses the LHCb data. Looking at the right panel, the corresponding neutrino fluxes show only mild sensitivity to the choice of scales.

B. k_T-Factorization

We have observed that introducing an additional k_T smearing improves the agreement of the collinear factorization prediction with data. This smearing effectively simulates intrinsic transverse momentum and soft-gluon emissions in the initial state. These effects are naturally included in the k_T-factorization approach due to the presence of the unintegrated gluon distribution function and the off-shell matrix element which depend on transverse momentum k_T. As discussed in Sec. III B, we are using a hybrid approach which utilizes an unintegrated PDF for the low-x gluon and an integrated PDF for the high-x gluon. This is because ultimately we are interested in the very forward region where one x is very small and the other very large.

As the basic setup we choose the unintegrated gluon distribution from the Kutak-Sapeta (`KS`) calculation [72] using the nonlinear evolution, and for the large-x we use the `CT14nlo` gluon. Since the `KS` gluon has been fitted to the HERA data using the leading order strong coupling constant, we use the same setup for the one power of strong coupling in the formula for the cross section. The second power of the coupling is taken at NLO consistent with the `CT14nlo` PDF used for large-x gluon. As before we are are modeling the hadronization using `Pythia` with the QCD-inspired color reconnection scheme. The results are shown in Fig. 5 by the blue curve. We observe that the calculation has the right shape in p_T but it significantly underestimates the experimental data. This was also observed in calculation of [46]. This is not totally unexpected since the off-shell partonic cross section used in k_T-factorization is effectively computed at the LO [55]. Therefore when compared with NLO collinear calculation it does not have virtual terms as well as final state gluon emissions from the quarks. It also has an off-shell gluon only on the small-x side. Given
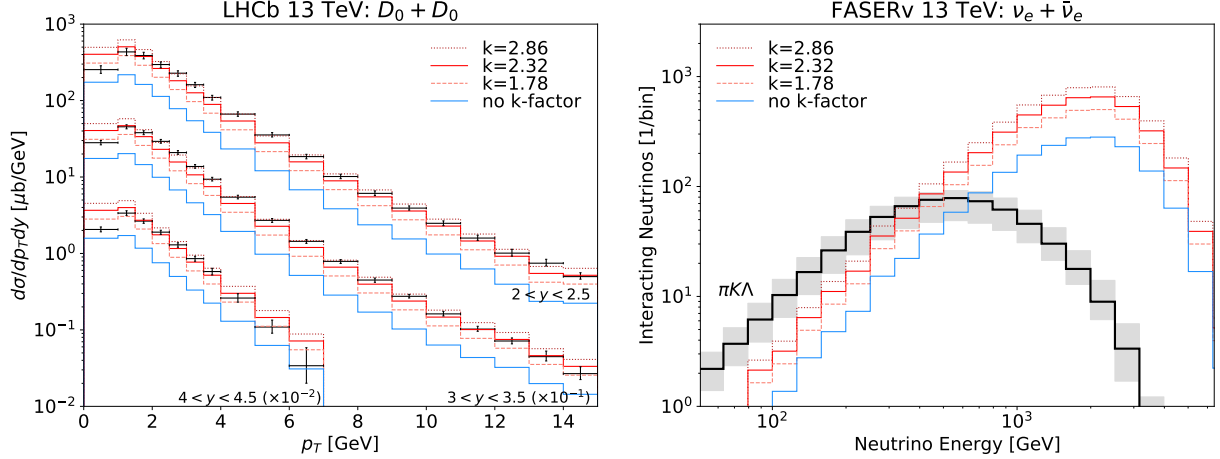
FIG. 5. **Normalization in k_T-Factorization:** Predictions using k_T-factorization before (blue) and after (red) applying an overall k-factor. These predictions use we use the `KS (non-linear)` unintegrated distribution for the low-x gluon, `CT14nlo` for the high-x gluon and use `Pythia` with the QCD-inspired color reconnection scheme to model fragmentation. See the main text for a detailed discussion.

that the NLO calculation in the collinear approach resulted in K-factor of the order of 2.5 with respect to the LO result, see e.g. [100], it is expected that the k_T-factorization will likely have large K-factor as well.

In order to get the normalization to agree with LHCb data, and therefore make our extrapolations from LHCb to FASERν more reliable, we introduce a normalization factor which we refer to as k-factor[2] in this calculation, determined by a fit to the data (with additional weights that ensure each rapidity bin contributes identically to the χ^2 measure). We find a best fit of $k = 2.32$; the resulting double-differential cross-section is illustrated by red line in Fig. 5. This is in excellent agreement with the LHCb data over the full p_T and rapidity range. This is encouraging since it means that the x dependence of the unintegrated gluon, correctly reproduces the rapidity dependence, and also the p_T dependence is correctly captured. We shall also see, that the k-factor does not change between the 7 and 13 TeV. We also determine an uncertainty of the fit, as illustrated by the orange and magenta curves in the same figure (using a rescaled χ^2 for this following the PDG procedure described in Refs. [80, 101]). These variations form a nice envelope around the data with a width of about a factor 2 at low values of p_T. The right panel in Fig. 5 shows the electron neutrino flux obtained in this approach. A similar size band is also obtained at FASERν, see right panel.

Next, we study the dependence of the results on the choice of the low-x unintegrated gluon distribution. In Fig. 6 we show our results for three choices of unintegrated PDFs: two choices for the `KS` gluon with linear evolution and with non-linear effects that describe saturation effects, and third choice of gluon from [73] obtained from the linear evolution including the resummation using the Ciafaloni-Colferai-Salam-Stasto (`CCSS`) approach [63]. We find that the prediction which includes saturation effects is in excellent agreement with the LHCb data over the full p_T range. In contrast, the linear cases overshoot the data at low p_T. However, given that the results include the k-factor effectively added by fitting as explained before, it is not possible to conclude at this moment about the importance of the saturation effects in the LHCb data. Looking at the right

---

[2] Traditionally a K-factor refers to a ratio between the NLO and LO calculations. Since here we are effectively using a normalization factor from lowest order to fit the data we refer to it as k-factor to distinguish it from the one usually defined in the literature.
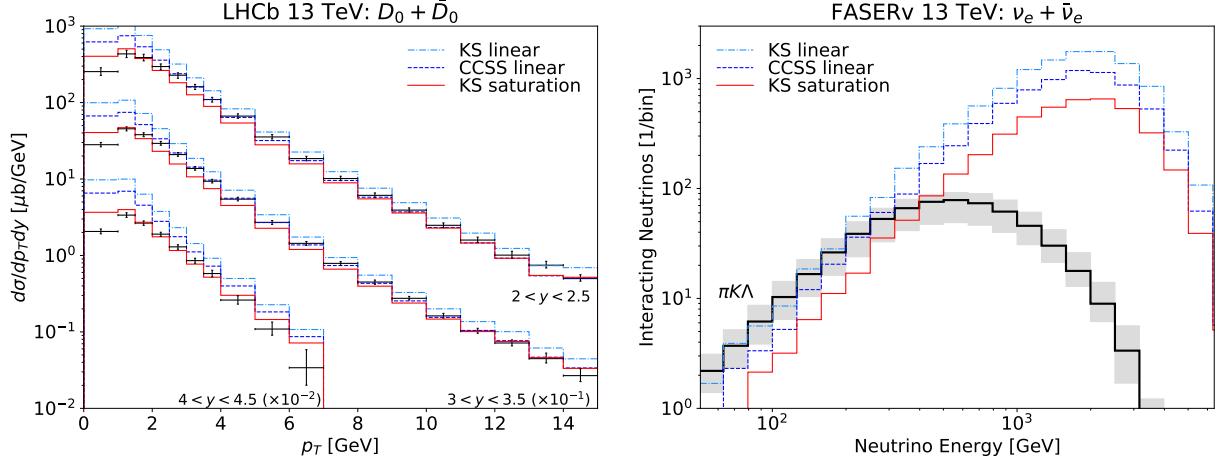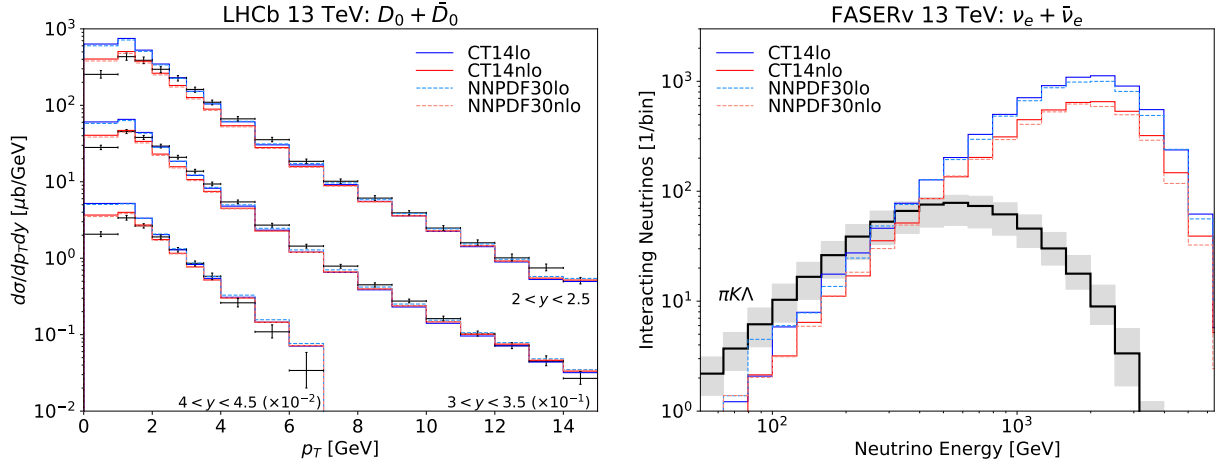
FIG. 6. **Low-x Gluon Distribution in k_T-Factorization:** Predictions using k_T-factorization using the `KS` (blue dot-dashed) and `CCSS` (blue dashed) unintegrated distribution with a purely linear evolution as well as the `KS` unintegrated distribution including non-linear effects that describe saturation effects (red solid) for the low-x gluon. All predictions use a constant k-factor of 2.32, the `CT14nlo` parton distribution function for the high-x gluon, use `Pythia` with the QCD-inspired color reconnection scheme to model fragmentation. See the main text for a detailed discussion.

FIG. 7. **High-x Gluon Distribution in k_T-Factorization:** Predictions using k_T-factorization based on different parton distribution of the high-x gluon. All predictions use a constant k-factor of 2.32, the `KS (non-linear)` unintegrated distribution for the low-x gluon and `Pythia` with the QCD-inspired color reconnection scheme to model fragmentation. See the main text for a detailed discussion.

panel, including saturation effects results in a reduction of the flux by a factor of approximately three compared to the linear case. This is due to the fact that the nonlinear effects are largest at very low p_T.

In Fig. 7, we explore the impact of the choice of integrated gluon distributions used for the high-x region, while keeping the unintegrated PDF with saturation for the low-x gluon fixed. We consider four different choices consisting of the `CT14` and `NNPDF30` distributions at both leading and next-to-leading order. Our results show that the next-to-leading order distributions provide a somewhat better description of the LHCb data. In contrast, the leading order distributions tend to overestimate the production rate at low p_T, leading to an increased neutrino flux. We observe
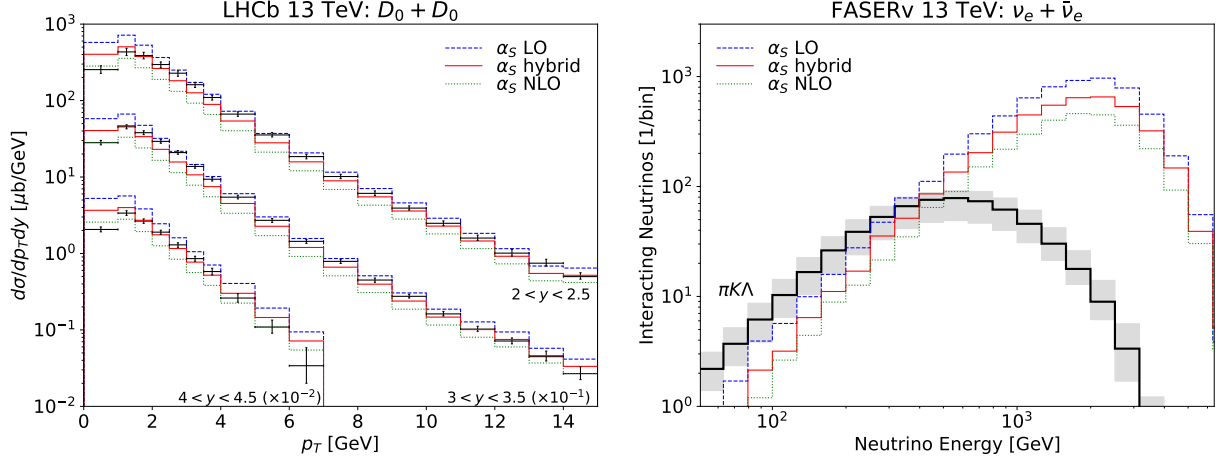
FIG. 8. **Strong Coupling in k_T-Factorization:** Predictions using k_T-factorization using different choices of the strong coupling: 'hybrid' (one power of coupling at LO and one power at NLO), 'LO' (both powers of strong coupling at LO) and 'NLO' (both powers of strong coupling at NLO corresponding to the large-x PDF). All predictions use a constant k-factor of 2.32, the `KS (non-linear)` unintegrated distribution for the low-x gluon, `CT14nlo` for the high-x gluon and `Pythia` with the QCD-inspired color reconnection scheme to model fragmentation. See the main text for a detailed discussion.
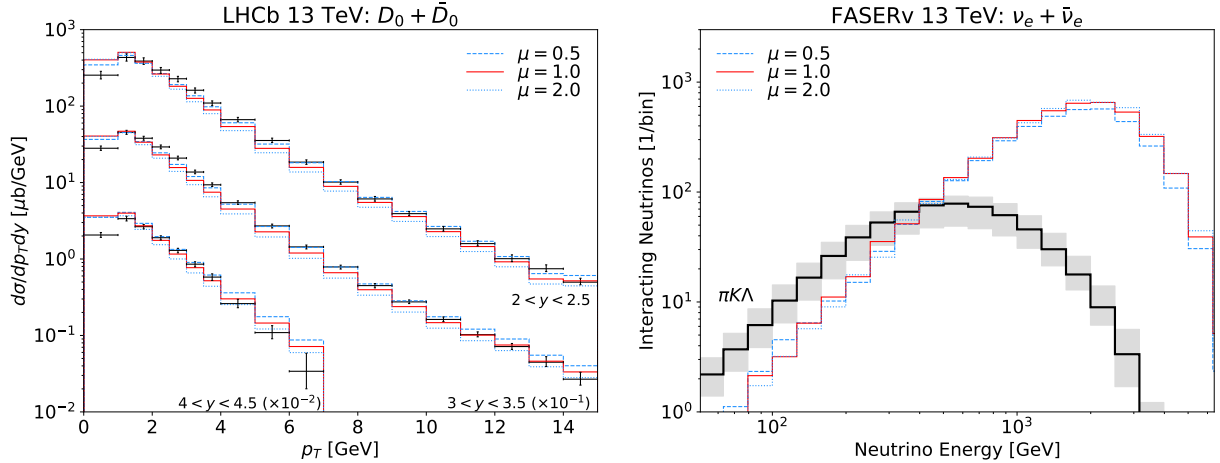
FIG. 9. **Scale Choice in k_T-Factorization:** Predictions using k_T-factorization using scale choice of $\mu \times \langle p_T^2 \rangle$, with $\langle p_T^2 \rangle = (p_{T1}^2 + p_{T2}^2)/2$ and values of $\mu = 0.5, 1.0, 2.0$ for dashed-blue, solid-red and dotted-blue curve respectively. All predictions use a constant k-factor of 2.32, the `KS (non-linear)` unintegrated distribution for the low-x gluon, `CT14nlo` for the high-x gluon and `Pythia` with the QCD-inspired color reconnection scheme to model fragmentation. See the main text for a detailed discussion.

small variations within the same order of distributions, with a corresponding uncertainty of about $20 - 25$ % at the peak of the flux. Therefore we choose the NLO PDFs in the calculation as our standard choice and for a better accuracy.

Next, in Fig. 8 we study the dependence of the k_T-factorization calculation on the choice of the order at which the strong coupling is taken as well as the value of Λ_{QCD}. Our standard choice is denoted by the 'hybrid' in Fig. 8. As mentioned previously this choice amounts to taking one power of the strong coupling in the leading order. This is consistent with the choice used in the fit used to extract the unintegrated `KS` gluon density in [72]. The second power of the strong coupling

is taken consistent with the choice of the large-x gluon PDF, in this case `CT14nlo` set. We also compare this with two other choices, one in which both powers of α_s are taken at leading order and one in which they are taken at NLO from `CT14nlo`, labeled as LO and NLO in Fig. 8, respectively. We see that these different choices give a moderate spread in the predictions. We remind here that we are using the same k-factor for all of these predictions, in order to isolate the dependence on the coupling choice. The shape in p_T is affected only modestly, mainly in the low p_T region. In the right panel in Fig. 8 we again show the spread of about factor of order 2 in the neutrino flux predictions.

Finally, we study the dependence on the variation of the scale in the large-x PDF and in the argument of the strong coupling. We vary the scale in the region $(0.5, 2.0)\langle p_T^2 \rangle$ where we define $\langle p_T^2 \rangle = (p_{T1}^2 + p_{T2}^2)/2$, and p_{T1}, p_{T2} are the transverse momenta of the produced quark and antiquark. The results are demonstrated in Fig. 9. We observe that the variation of scales has very little impact on both the p_T dependent cross section at LHCb as well as on the neutrino results at FASERν.

C.   Comparison of Approaches

Based on the previous discussion, we identify central predictions for both factorization approaches. In particular, we consider the following configuration

- **collinear factorization at NLO** with `CT14nlo` for the gluon parton distribution, renormalization scale $\mu_R = 1.75 \, m_T$, factorization scale $\mu_F = 1.25 \, m_T$, a k_T smearing with $\langle k_T \rangle = 1.5$ GeV, and fragmentation modelled with `Pythia` with the QCD-inspired color reconnection scheme

- k_T-**factorization** using `KS` unintegrated distribution for the low-x gluon including saturation effects, the `CT14nlo` parton distribution for the high-x gluon, a k-factor of 2.32 and fragmentation modelled with `Pythia` with the QCD-inspired color reconnection scheme

In Fig. 10, we compare the corresponding distributions from both approaches. We note that k_T-factorization with saturation gives slightly better description of the p_T shape of the LHCb data than the NLO case. However, we again remind the reader, that this has to be taken with caution since this calculation includes the fitted k-factor which is not needed for the NLO collinear approach. We find that both approaches give good description of $D^0 + \bar{D}^0$ data but when compared with LHCb data for $D^+ + D^-$, and for $D_s + D_s^-$, the low p_T region is overestimated. We show distributions as a function of rapidity for different p_T regions, and we find that NLO and k_T-factorization with saturation give similar values for central rapidity, but they differ at large rapidity, by about a factor of 2, especially for $0 < p_T < 0.5$ region. For large values of p_T, this difference is reduced.

In Fig. 11, we also show comparison of both approaches with the LHCb data at 7 TeV, and the description is very good in both cases. It should be stressed that the used scales for the NLO calculation and the k-factor for k_T-factorization at 7 TeV are the same as extracted from 13 TeV data. As mentioned previously, this is encouraging since it means that the energy dependence of the data, which is driven mainly by the x evolution of the unintegrated gluon density is captured correctly. The latter one has been taken from the resummed approaches [63, 74, 77] which aim to reproduce both small-x and collinear dynamics.

The neutrino flux obtained using both QCD approaches is presented in Fig. 12. The upper row shows the number of interacting neutrinos in FASERν operating during LHC Run 3 with an integrated luminosity of 150 fb^{-1} while the bottom row shows the neutrino events rate at FLARE at the FPF during the HL-LHC with a luminosity of 3 ab^{-1}. The three columns correspond to the three neutrino flavors. The shape of the neutrino flux remains similar for all neutrino flavors in both
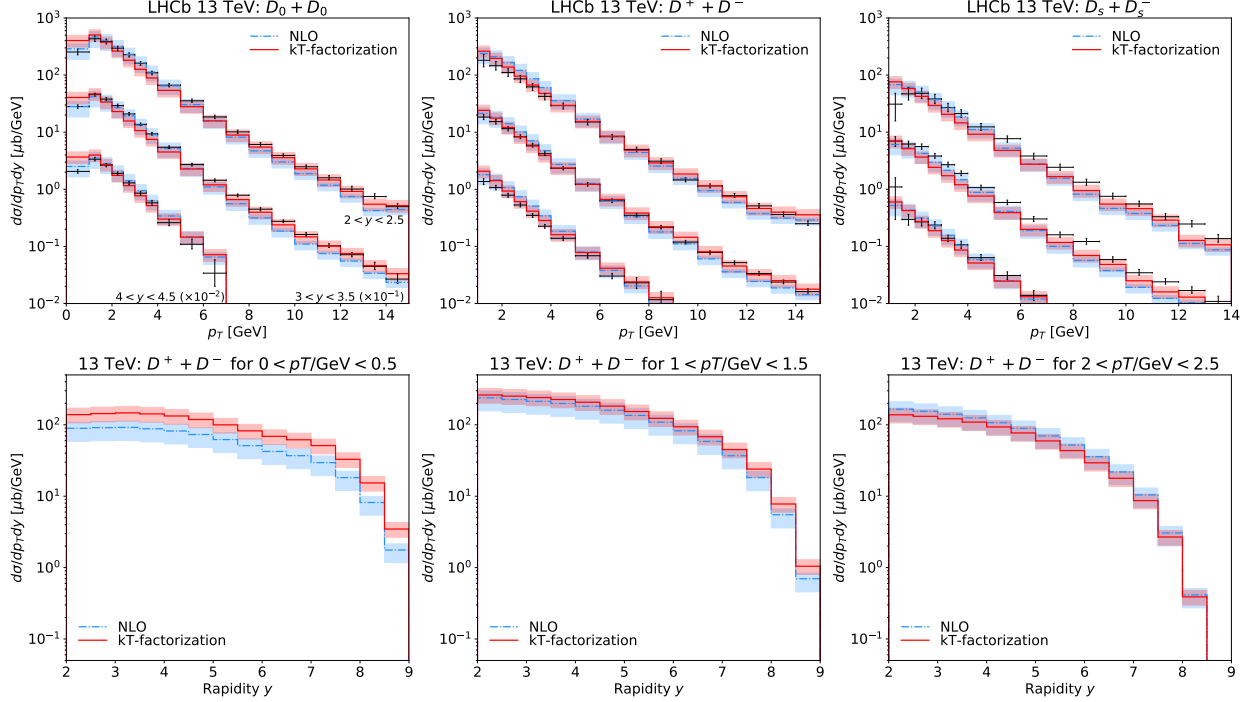
FIG. 10. **Comparison of Charm Hadron Distribution at 13 TeV:** Predictions using collinear factorization at NLO and k_T-factorization. The shaded band around the NLO predictions corresponds to the scale variations shown in Fig. 4 while the shaded band around the k_T-factorization prediction corresponds to a varation of the k-factor as shown in Fig. 5. In the top row, we show the p_T distributions for all three charmed mesons in comparison to LHCb data. The bottom row show the rapidity distribution for $D^{\pm}$ mesons in three transverse momentum regions.
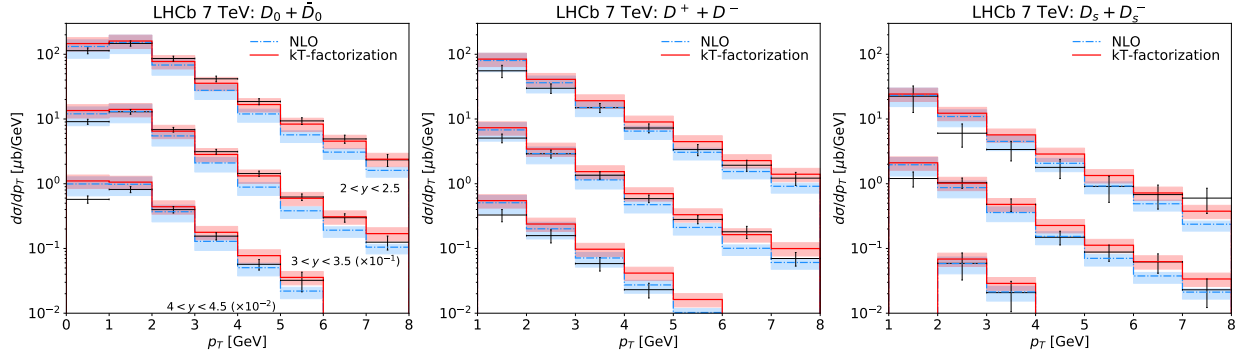
FIG. 11. **Comparison of Charm Hadron Distribution at 7 TeV:** Transverse momentum distributions for all three charmed mesons in comparison to 7 TeV LHCb data using the same collinear factorization at NLO and k_T-factorization setups as in Fig. 10.

approaches, with the NLO contribution slightly lower than that of the k_T-factorization. However, the two approaches are very close and fall within the range of uncertainty, which is approximately a factor of two. The black lines represent the contribution to the neutrino flux from decays of light hadrons. Notably, we find that the dominant contribution to neutrinos occurs above 500 GeV for ν_e and above 1 TeV for ν_μ. Detecting ν_τ would serve as a direct test of charm production, as there is no contribution from pions and kaons decays.
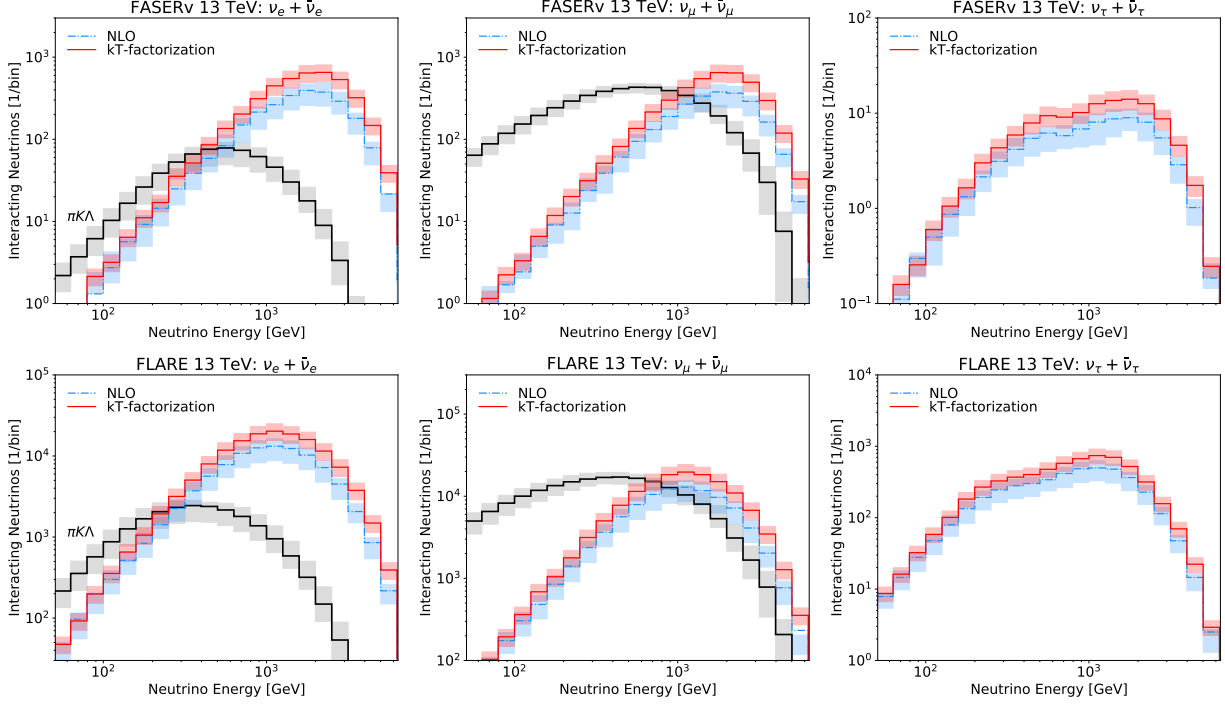
FIG. 12. **Comparison of Forward Neutrino Distributions:** Forward neutrino flux predictions using the same collinear factorization at NLO and k_T-factorization setups as in Fig. 10. The energy spectra of neutrinos interacting in FASERν at Run 3 of the LHC are shown in the top row for all three neutrino flavors. Similar distributions for proposed FLARE detector at FPF during the HL-LHC era are shown in the bottom row.

Based on our calculation, we predict that FASERν during LHC Run 3 is expected to observe approximately 4000 ν_e, 4000 ν_μ, and 120 ν_τ charge current interactions originating from decays of charm hadrons. The FPF, proposed to house larger neutrino detectors during the HL-LHC era, aims to record a significantly larger sample of neutrino interaction events [21, 22]. Specifically, we can see that the FLARE detector housed within the FPF will detect approximately 1.4×10^5 ν_e, 1.4×10^5 ν_μ, and 6000 ν_τ. This substantial increase in statistics will enable FPF experiments to conduct more detailed tests on forward charm production and provide the necessary data to distinguish between different predictions.

VI. CONCLUSION

Forward charm production at hadron colliders has long been recognized as an intriguing tool for probing the strong interaction. However, until recently, it has remained beyond the reach of the existing LHC experiments. This situation is now changing with the start of operation of the FASERν and SND@LHC experiments, which are strategically positioned in the far-forward direction of the LHC and specifically designed to detect collider neutrinos. Many of these neutrinos originate from the decay of charm hadrons, presenting a unique opportunity to investigate forward charm production. Together, FASERν and SND@LHC are projected to observe approximately ten thousand neutrinos during the LHC's Run 3, spanning from 2022 to 2025. Looking forward, a continuation of this collider neutrino program is envisioned for the HL-LHC era from 2029 to 2042: by utilizing larger detectors situated in the FPF it will be possible to detect millions of collider

neutrinos.

In order to predict neutrino fluxes from charmed mesons in these forward neutrino experiments, we have examined two distinct perturbative QCD approaches for calculating charm quark pair production cross-sections in proton-proton collisions: collinear factorization at NLO and the k_T-factorization approach. Subsequently, we have modeled their hadronization using `Pythia`, enabling us to derive the distributions of charmed hadrons. These distributions have been compared to measurements by LHCb, and based on this comparison, we have made predictions for the corresponding forward neutrino fluxes at the LHC neutrino experiments.

We have obtained final predictions using the two different formalisms. For the collinear factorization at NLO approach, we have employed the `CT14nlo` parton distribution functions with a renormalization scale of $\mu_R = 1.75\ m_T$ and a factorization scale of $\mu_F = 1.25\ m_T$, determined through a fit to data. To improve the shape of the charm hadron distribution and align it with LHCb measurements, we have implemented a k_T smearing with $\langle k_T \rangle = 1.5$ GeV. In the k_T-factorization approach, our central prediction incorporates the `KS` unintegrated distribution with a non-linear evolution for the low-x gluon, and the `CT14nlo` distribution for large-x gluons. Additionally, we introduce a constant k-factor of 2.32, determined by fitting the overall normalization to the LHCb data. The need for the inclusion of the normalization k-factor in k_T-factorization approach likely stems from the fact that the off-shell partonic cross section for production of heavy quarks is only available at lowest order. Higher orders of the off-shell partonic cross section will need to be computed, and possibly resummed, to obtain more precise predictions. With this caveat in mind we observe, that both QCD approaches provide a good description of the LHCb data, exhibiting similar energy dependence in the neutrino flux with slightly different overall normalizations, which can be attributed to the specific QCD parameter choices. We have further examined the impact of systematically varying the underlying QCD parameters, such as scale selection, parton distribution function choices, and fragmentation modeling, on these predictions.

Notably, we have emphasized the significance of accurately modeling charm fragmentation. We found that existing fragmentation functions obtained from lepton collider data are insufficient in describing various observed effects in forward and low-p_T charm data at hadron collisions. Some of these observations are attributed to the hadronization process of charm quarks with the remnants of the colliding beams, which holds particular importance in the forward direction relevant to the LHC neutrino experiments. To address these challenges, we have employed the string fragmentation model implemented in `Pythia`, resulting in a more realistic representation of hadronization. Indeed, our findings demonstrate a significantly enhanced flux of forward neutrinos compared to using established fragmentation functions, underscoring the importance of utilizing an accurate fragmentation modeling. However, we also note that the topic of forward charm hadronization warrants further theoretical investigation.

Using our best-fit QCD parameters, we have shown predictions for neutrino fluxes of all three flavors for the ongoing FASER experiment as well as the proposed FLARE detector at the FPF and compared them against those from the decay of lighter mesons. We find that, depending on the choice of QCD scheme, the electron neutrino flux from charmed mesons dominates over those from pions and kaons starting at neutrino energies between 400 and 500 GeV. Furthermore, muon neutrinos from charmed meson decay become comparable to those from pion and kaon decays at energies above 1 TeV for both QCD approaches. Tau neutrinos, produced exclusively from heavy meson decays, provide a background-free channel to investigate heavy meson QCD. Our models predict between 4000 and 6000 charged current tau neutrino interactions at FLARE with energies around 1 TeV, depending on whether one uses the collinear NLO scheme or the k_T-factorization scheme respectively.

The first observation of collider neutrinos at FASER [37] heralds the opening of a new fron-

tier towards significantly improved understanding of forward QCD. Further measurements at both FASER and SND@LHC will provide a unique opportunity to gather valuable information about small-x QCD, validity of k_T-factorization and NLO collinear approach, and validity of different hadronic fragmentation scenarios at forward rapidities. In the future, the planned experiments at the FPF, with significantly improved statistics, will become the ideal place to unravel these most important facets of QCD. In addition, we expect that measurements of the forward neutrino production at the LHC will provide valuable inputs for estimating the prompt neutrino flux, reducing its theoretical uncertainties and thus providing a better understanding of the main background for the detection of ultra-high energy neutrinos be it from extragalactic astrophysical sources or from beyond standard model physics including dark matter decays and annihilation.

VII. ACKNOWLEDGMENT

[1] **H1, ZEUS** Collaboration, F. D. Aaron *et al.*, "Combined Measurement and QCD Analysis of the Inclusive e+- p Scattering Cross Sections at HERA," *JHEP* **01** (2010) 109, `arXiv:0911.0884 [hep-ex]`.

[2] A. D. Martin, M. G. Ryskin, and A. M. Stasto, "Prompt neutrinos from atmospheric $c\bar{c}$ and $b\bar{b}$ production and the gluon at very small x," *Acta Phys. Polon. B* **34** (2003) 3273–3304, `arXiv:hep-ph/0302140`.

[3] L. V. Gribov, E. M. Levin, and M. G. Ryskin, "Semihard Processes in QCD," *Phys. Rept.* **100** (1983) 1–150.

[4] A. Bhattacharya, R. Enberg, M. H. Reno, I. Sarcevic, and A. Stasto, "Perturbative charm production and the prompt atmospheric neutrino flux in light of RHIC and LHC," *JHEP* **06** (2015) 110, `arXiv:1502.01076 [hep-ph]`.

[5] R. Gauld, J. Rojo, L. Rottoli, and J. Talbert, "Charm production in the forward region: constraints on the small-x gluon and backgrounds for neutrino astronomy," *JHEP* **11** (2015) 009, `arXiv:1506.08025 [hep-ph]`.

[6] M. V. Garzelli, S. Moch, and G. Sigl, "Lepton fluxes from atmospheric charm revisited," *JHEP* **10** (2015) 115, `arXiv:1507.01570 [hep-ph]`.

[7] **IceCube** Collaboration, R. Abbasi *et al.*, "The IceCube high-energy starting event sample: Description and flux characterization with 7.5 years of data," *Phys. Rev. D* **104** (2021) 022002, `arXiv:2011.03545 [astro-ph.HE]`.

[8] **ATLAS** Collaboration, G. Aad *et al.*, "Measurement of $D^{*\pm}$, $D^{\pm}$ and $D_s^{\pm}$ meson production cross sections in pp collisions at $\sqrt{s} = 7$ TeV with the ATLAS detector," *Nucl. Phys. B* **907** (2016) 717–763, `arXiv:1512.02913 [hep-ex]`.

[9] **CMS** Collaboration, A. M. Sirunyan *et al.*, "Nuclear modification factor of D^0 mesons in PbPb collisions at $\sqrt{s_{NN}} = 5.02$ TeV," *Phys. Lett. B* **782** (2018) 474–496, arXiv:1708.04962 [nucl-ex].

[10] **CMS** Collaboration, A. Tumasyan *et al.*, "Measurement of prompt open-charm production cross sections in proton-proton collisions at $\sqrt{s} = 13$ TeV," *JHEP* **11** (2021) 225, arXiv:2107.01476 [hep-ex].

[11] **ALICE** Collaboration, S. Acharya *et al.*, "Measurement of D-meson production at mid-rapidity in pp collisions at $\sqrt{s} = 7$ TeV," *Eur. Phys. J. C* **77** (2017) no. 8, 550, arXiv:1702.00766 [hep-ex].

[12] **ALICE** Collaboration, S. Acharya *et al.*, "Measurement of D^0, D^+, D^{*+} and D_s^+ production in pp collisions at $\sqrt{s} = 5.02$ TeV with ALICE," *Eur. Phys. J. C* **79** (2019) no. 5, 388, arXiv:1901.07979 [nucl-ex].

[13] **LHCb** Collaboration, R. Aaij *et al.*, "Prompt charm production in pp collisions at sqrt(s)=7 TeV," *Nucl. Phys. B* **871** (2013) 1–20, arXiv:1302.2864 [hep-ex].

[14] **LHCb** Collaboration, R. Aaij *et al.*, "Measurements of prompt charm production cross-sections in *pp* collisions at $\sqrt{s} = 13$ TeV," *JHEP* **03** (2016) 159, arXiv:1510.01707 [hep-ex]. [Erratum: JHEP 09, 013 (2016), Erratum: JHEP 05, 074 (2017)].

[15] **LHCb** Collaboration, R. Aaij *et al.*, "Measurements of prompt charm production cross-sections in pp collisions at $\sqrt{s} = 5$ TeV," *JHEP* **06** (2017) 147, arXiv:1610.02230 [hep-ex].

[16] **FASER** Collaboration, H. Abreu *et al.*, "Detecting and Studying High-Energy Collider Neutrinos with FASER at the LHC," *Eur. Phys. J. C* **80** (2020) no. 1, 61, arXiv:1908.02310 [hep-ex].

[17] **FASER** Collaboration, H. Abreu *et al.*, "Technical Proposal: FASERnu," arXiv:2001.03073 [physics.ins-det].

[18] **SHiP** Collaboration, C. Ahdida *et al.*, "SND@LHC," arXiv:2002.08722 [physics.ins-det].

[19] C. Ahdida *et al.*, "SND@LHC - Scattering and Neutrino Detector at the LHC," tech. rep., CERN, Geneva, Jan, 2021. https://cds.cern.ch/record/2750060.

[20] R. Mammen Abraham *et al.*, "Forward Physics Facility - Snowmass 2021 Letter of Interest,".

[21] L. A. Anchordoqui *et al.*, "The Forward Physics Facility: Sites, experiments, and physics potential," *Phys. Rept.* **968** (2022) 1–50, arXiv:2109.10905 [hep-ph].

[22] J. L. Feng, F. Kling, M. H. Reno, J. Rojo, D. Soldin, *et al.*, "The Forward Physics Facility at the High-Luminosity LHC," arXiv:2203.05090 [hep-ex].

[23] **LHCf** Collaboration, O. Adriani *et al.*, "Measurement of forward photon production cross-section in proton–proton collisions at $\sqrt{s} = 13$ TeV with the LHCf detector," *Phys. Lett. B* **780** (2018) 233–239, arXiv:1703.07678 [hep-ex].

[24] **LHCf** Collaboration, O. Adriani *et al.*, "Measurement of energy flow, cross section and average inelasticity of forward neutrons produced in $\sqrt{s} = 13$ TeV proton-proton collisions with the LHCf Arm2 detector," *JHEP* **07** (2020) 016, arXiv:2003.02192 [hep-ex].

[25] **EAS-MSU, IceCube, KASCADE Grande, NEVOD-DECOR, Pierre Auger, SUGAR, Telescope Array, Yakutsk EAS Array** Collaboration, L. Cazon, "Working Group Report on the Combined Analysis of Muon Density Measurements from Eight Air Shower Experiments," *PoS* **ICRC2019** (2020) 214, arXiv:2001.07508 [astro-ph.HE].

[26] L. A. Anchordoqui, C. G. Canal, F. Kling, S. J. Sciutto, and J. F. Soriano, "An explanation of the muon puzzle of ultrahigh-energy cosmic rays and the role of the Forward Physics Facility for model improvement," *JHEAp* **34** (2022) 19–32, arXiv:2202.03095 [hep-ph].

[27] A. De Rujula, E. Fernandez, and J. J. Gomez-Cadenas, "Neutrino fluxes at future hadron colliders," *Nucl. Phys. B* **405** (1993) 80–108.

[28] **FASER** Collaboration, H. Abreu *et al.*, "First neutrino interaction candidates at the LHC," *Phys. Rev. D* **104** (2021) no. 9, L091101, arXiv:2105.06197 [hep-ex].

[29] **FASER** Collaboration, A. Ariga *et al.*, "Letter of Intent for FASER: ForwArd Search ExpeRiment at the LHC," arXiv:1811.10243 [physics.ins-det].

[30] **FASER** Collaboration, A. Ariga *et al.*, "Technical Proposal for FASER: ForwArd Search ExpeRiment at the LHC," arXiv:1812.09139 [physics.ins-det].

[31] **FASER** Collaboration, H. Abreu *et al.*, "The FASER Detector," arXiv:2207.11427 [physics.ins-det].

[32] J. L. Feng, I. Galon, F. Kling, and S. Trojanowski, "ForwArd Search ExpeRiment at the LHC," *Phys. Rev. D* **97** (2018) no. 3, 035001, arXiv:1708.09389 [hep-ph].

[33] J. L. Feng, I. Galon, F. Kling, and S. Trojanowski, "Dark Higgs bosons at the ForwArd Search ExpeRiment," *Phys. Rev. D* **97** (2018) no. 5, 055034, `arXiv:1710.09387 [hep-ph]`.

[34] F. Kling and S. Trojanowski, "Heavy Neutral Leptons at FASER," *Phys. Rev. D* **97** (2018) no. 9, 095016, `arXiv:1801.08947 [hep-ph]`.

[35] J. L. Feng, I. Galon, F. Kling, and S. Trojanowski, "Axionlike particles at FASER: The LHC as a photon beam dump," *Phys. Rev. D* **98** (2018) no. 5, 055021, `arXiv:1806.02348 [hep-ph]`.

[36] **FASER** Collaboration, A. Ariga *et al.*, "FASER's physics reach for long-lived particles," *Phys. Rev. D* **99** (2019) no. 9, 095011, `arXiv:1811.12522 [hep-ph]`.

[37] **FASER** Collaboration, H. Abreu *et al.*, "First Direct Observation of Collider Neutrinos with FASER at the LHC," `arXiv:2303.14185 [hep-ex]`.

[38] **SND@LHC** Collaboration, C. L. Albanese and J. C. Brauer, "Observation of collider muon neutrinos with the SND@LHC experiment," `arXiv:2305.09383 [hep-ex]`.

[39] F. Kling and L. J. Nevay, "Forward neutrino fluxes at the LHC," *Phys. Rev. D* **104** (2021) no. 11, 113008, `arXiv:2105.08270 [hep-ph]`.

[40] W. Bai, M. Diwan, M. V. Garzelli, Y. S. Jeong, and M. H. Reno, "Far-forward neutrinos at the Large Hadron Collider," *JHEP* **06** (2020) 032, `arXiv:2002.03012 [hep-ph]`.

[41] W. Bai, M. Diwan, M. V. Garzelli, Y. S. Jeong, F. K. Kumar, and M. H. Reno, "Parton distribution function uncertainties in theoretical predictions for far-forward tau neutrinos at the Large Hadron Collider," *JHEP* **06** (2022) 148, `arXiv:2112.11605 [hep-ph]`.

[42] W. Bai, M. Diwan, M. V. Garzelli, Y. S. Jeong, K. Kumar, and M. H. Reno, "Forward production of prompt neutrinos from charm in the atmosphere and at high energy colliders," `arXiv:2212.07865 [hep-ph]`.

[43] Y. S. Jeong, W. Bai, M. Diwan, M. V. Garzelli, and M. H. Reno, "Prompt tau neutrinos at the LHC," *PoS* **NuFact2019** (2020) 096.

[44] Y. S. Jeong, W. Bai, M. Diwan, M. V. Garzelli, F. K. Kumar, and M. H. Reno, "Neutrinos from charm: forward production at the LHC and in the atmosphere," *PoS* **ICRC2021** (2021) 1218, `arXiv:2107.01178 [hep-ph]`.

[45] W. Bai, M. V. Diwan, M. V. Garzelli, Y. S. Jeong, K. Kumar, and M. H. Reno, "Prompt electron and tau neutrinos and antineutrinos in the forward region at the LHC," *JHEAp* **34** (2022) 212–216, `arXiv:2203.07212 [hep-ph]`.

[46] R. Maciula and A. Szczurek, "Far-forward production of charm mesons and neutrinos at forward physics facilities at the LHC and the intrinsic charm in the proton," *Phys. Rev. D* **107** (2023) no. 3, 034002, `arXiv:2210.08890 [hep-ph]`.

[47] R. Maciuła and A. Szczurek, "Intrinsic charm in the nucleon and charm production at large rapidities in collinear, hybrid and k$_T$-factorization approaches," *JHEP* **10** (2020) 135, `arXiv:2006.16021 [hep-ph]`.

[48] M. Cacciari, M. Greco, and P. Nason, "The P(T) spectrum in heavy flavor hadroproduction," *JHEP* **05** (1998) 007, `arXiv:hep-ph/9803400`.

[49] M. Cacciari, S. Frixione, and P. Nason, "The p(T) spectrum in heavy flavor photoproduction," *JHEP* **03** (2001) 006, `arXiv:hep-ph/0102134`.

[50] M. R. Whalley, D. Bourilkov, and R. C. Group, "The Les Houches accord PDFs (LHAPDF) and LHAGLUE," in *HERA and the LHC: A Workshop on the Implications of HERA and LHC Physics*, pp. 575–581. 8, 2005. `arXiv:hep-ph/0508110`.

[51] A. Buckley, J. Ferrando, S. Lloyd, K. Nordström, B. Page, M. Rüfenacht, M. Schönherr, and G. Watt, "LHAPDF6: parton density access in the LHC precision era," *Eur. Phys. J. C* **75** (2015) 132, `arXiv:1412.7420 [hep-ph]`.

[52] S. Dulat, T.-J. Hou, J. Gao, M. Guzzi, J. Huston, P. Nadolsky, J. Pumplin, C. Schmidt, D. Stump, and C. P. Yuan, "New parton distribution functions from a global analysis of quantum chromodynamics," *Phys. Rev. D* **93** (2016) no. 3, 033006, `arXiv:1506.07443 [hep-ph]`.

[53] V. Bertone, R. Gauld, and J. Rojo, "Neutrino Telescopes as QCD Microscopes," *JHEP* **01** (2019) 217, `arXiv:1808.02034 [hep-ph]`.

[54] **PROSA** Collaboration, O. Zenaiev, M. V. Garzelli, K. Lipka, S. O. Moch, A. Cooper-Sarkar, F. Olness, A. Geiser, and G. Sigl, "Improved constraints on parton distributions using LHCb, ALICE and HERA heavy-flavour measurements and implications for the predictions for prompt

atmospheric-neutrino fluxes," *JHEP* **04** (2020) 118, `arXiv:1911.13164 [hep-ph]`.

[55] S. Catani, M. Ciafaloni, and F. Hautmann, "High-energy factorization and small x heavy flavor production," *Nucl. Phys. B* **366** (1991) 135–188.

[56] S. Catani, M. Ciafaloni, and F. Hautmann, "Gluon Contributions to Small x Heavy Flavor Production," *Phys. Lett. B* **242** (1990) 97–102.

[57] J. C. Collins and R. K. Ellis, "Heavy quark production in very high-energy hadron collisions," *Nucl. Phys. B* **360** (1991) 3–30.

[58] J. Collins, *Foundations of perturbative QCD*, vol. 32. Cambridge University Press, 11, 2013.

[59] P. Kotko, K. Kutak, C. Marquet, E. Petreska, S. Sapeta, and A. van Hameren, "Improved TMD factorization for forward dijet production in dilute-dense hadronic collisions," *JHEP* **09** (2015) 106, `arXiv:1503.03421 [hep-ph]`.

[60] I. Balitsky and A. Tarasov, "Rapidity evolution of gluon TMD from low to moderate x," *JHEP* **10** (2015) 017, `arXiv:1505.02151 [hep-ph]`.

[61] E. A. Kuraev, L. N. Lipatov, and V. S. Fadin, "The Pomeranchuk Singularity in Nonabelian Gauge Theories," *Sov. Phys. JETP* **45** (1977) 199–204.

[62] I. I. Balitsky and L. N. Lipatov, "The Pomeranchuk Singularity in Quantum Chromodynamics," *Sov. J. Nucl. Phys.* **28** (1978) 822–829.

[63] M. Ciafaloni, D. Colferai, G. P. Salam, and A. M. Stasto, "Renormalization group improved small x Green's function," *Phys. Rev. D* **68** (2003) 114003, `arXiv:hep-ph/0307188`.

[64] L. D. McLerran and R. Venugopalan, "Gluon distribution functions for very large nuclei at small transverse momentum," *Phys. Rev. D* **49** (1994) 3352–3355, `arXiv:hep-ph/9311205`.

[65] L. D. McLerran and R. Venugopalan, "Computing quark and gluon distribution functions for very large nuclei," *Phys. Rev. D* **49** (1994) 2233–2241, `arXiv:hep-ph/9309289`.

[66] J. Jalilian-Marian, A. Kovner, A. Leonidov, and H. Weigert, "The Wilson renormalization group for low x physics: Towards the high density regime," *Phys. Rev. D* **59** (1998) 014014, `arXiv:hep-ph/9706377`.

[67] J. Jalilian-Marian, A. Kovner, A. Leonidov, and H. Weigert, "The BFKL equation from the Wilson renormalization group," *Nucl. Phys. B* **504** (1997) 415–431, `arXiv:hep-ph/9701284`.

[68] E. Iancu, A. Leonidov, and L. D. McLerran, "Nonlinear gluon evolution in the color glass condensate. 1.," *Nucl. Phys. A* **692** (2001) 583–645, `arXiv:hep-ph/0011241`.

[69] E. Ferreiro, E. Iancu, A. Leonidov, and L. McLerran, "Nonlinear gluon evolution in the color glass condensate. 2.," *Nucl. Phys. A* **703** (2002) 489–538, `arXiv:hep-ph/0109115`.

[70] I. Balitsky, "Operator expansion for high-energy scattering," *Nucl. Phys. B* **463** (1996) 99–160, `arXiv:hep-ph/9509348`.

[71] Y. V. Kovchegov, "Small x F(2) structure function of a nucleus including multiple pomeron exchanges," *Phys. Rev. D* **60** (1999) 034008, `arXiv:hep-ph/9901281`.

[72] K. Kutak and S. Sapeta, "Gluon saturation in dijet production in p-Pb collisions at Large Hadron Collider," *Phys. Rev. D* **86** (2012) 094043, `arXiv:1205.5035 [hep-ph]`.

[73] W. Li and A. M. Stasto, "Structure functions from renormalization group improved small x evolution," *Eur. Phys. J. C* **82** (2022) no. 6, 562, `arXiv:2201.10579 [hep-ph]`.

[74] J. Kwiecinski, A. D. Martin, and A. M. Stasto, "A Unified BFKL and GLAP description of F2 data," *Phys. Rev. D* **56** (1997) 3991–4006, `arXiv:hep-ph/9703445`.

[75] K. Kutak and J. Kwiecinski, "Screening effects in the ultrahigh-energy neutrino interactions," *Eur. Phys. J. C* **29** (2003) 521, `arXiv:hep-ph/0303209`.

[76] K. Kutak and A. M. Stasto, "Unintegrated gluon distribution from modified BK equation," *Eur. Phys. J. C* **41** (2005) 343–351, `arXiv:hep-ph/0408117`.

[77] M. Ciafaloni, D. Colferai, D. Colferai, G. P. Salam, and A. M. Stasto, "Extending QCD perturbation theory to higher energies," *Phys. Lett. B* **576** (2003) 143–151, `arXiv:hep-ph/0305254`.

[78] M. Lisovyi, A. Verbytskyi, and O. Zenaiev, "Combined analysis of charm-quark fragmentation-fraction measurements," *Eur. Phys. J. C* **76** (2016) no. 7, 397, `arXiv:1509.01061 [hep-ex]`.

[79] C. Peterson, D. Schlatter, I. Schmitt, and P. M. Zerwas, "Scaling Violations in Inclusive e+ e- Annihilation Spectra," *Phys. Rev. D* **27** (1983) 105.

[80] **Particle Data Group** Collaboration, P. A. Zyla *et al.*, "Review of Particle Physics," *PTEP* **2020** (2020) no. 8, 083C01.

[81] **WA82** Collaboration, M. Adamovich *et al.*, "Study of D+ and D- Feynman's x distributions in pi-nucleus interactions at the SPS," *Phys. Lett. B* **305** (1993) 402–406.

[82] **E769** Collaboration, G. A. Alves *et al.*, "Enhanced leading production of D+- and D*+- in 250-GeV pi+- - nucleon interactions," *Phys. Rev. Lett.* **72** (1994) 812–815. [Erratum: Phys.Rev.Lett. 72, 1946 (1994)].

[83] **E791** Collaboration, E. M. Aitala *et al.*, "Asymmetries between the production of D^+ and D^- mesons from 500-GeV/c π^- - nucleon interactions as a function of x_F and p_t^2," *Phys. Lett. B* **371** (1996) 157–162, `arXiv:hep-ex/9601001`.

[84] E. Norrbin and T. Sjostrand, "Production mechanisms of charm hadrons in the string model," *Phys. Lett. B* **442** (1998) 407–416, `arXiv:hep-ph/9809266`.

[85] **ALICE** Collaboration, S. Acharya *et al.*, "Λ_c^+ production in pp collisions at $\sqrt{s} = 7$ TeV and in p-Pb collisions at $\sqrt{s_{NN}} = 5.02$ TeV," *JHEP* **04** (2018) 108, `arXiv:1712.09581 [nucl-ex]`.

[86] **ALICE** Collaboration, S. Acharya *et al.*, "Λ_c^+ production in *pp* and in *p*-Pb collisions at $\sqrt{s_{NN}}$=5.02 TeV," *Phys. Rev. C* **104** (2021) no. 5, 054905, `arXiv:2011.06079 [nucl-ex]`.

[87] **ALICE** Collaboration, S. Acharya *et al.*, "Measurement of Prompt D^0, Λ_c^+, and $\Sigma_c^{0,++}(2455)$ Production in Proton–Proton Collisions at $\sqrt{s} = 13$ TeV," *Phys. Rev. Lett.* **128** (2022) no. 1, 012001, `arXiv:2106.08278 [hep-ex]`.

[88] **CMS** Collaboration, A. M. Sirunyan *et al.*, "Production of Λ_c^+ baryons in proton-proton and lead-lead collisions at $\sqrt{s_{NN}} = 5.02$ TeV," *Phys. Lett. B* **803** (2020) 135328, `arXiv:1906.03322 [hep-ex]`.

[89] **ALICE** Collaboration, Y. Bailung, "Measurement of D-meson production as a function of charged-particle multiplicity in proton–proton collisions at $\sqrt{s} = 13$ TeV with ALICE at the LHC," *PoS* **LHCP2021** (2021) 190, `arXiv:2109.07992 [hep-ex]`.

[90] **ALICE** Collaboration, J. E. Mdhluli, "Correlation of heavy-flavour hadron production and charged-particle multiplicity in pp collisions measured by ALICE," `arXiv:2210.16516 [hep-ex]`.

[91] T. Sjostrand, S. Mrenna, and P. Z. Skands, "PYTHIA 6.4 Physics and Manual," *JHEP* **05** (2006) 026, `arXiv:hep-ph/0603175`.

[92] T. Sjöstrand, S. Ask, J. R. Christiansen, R. Corke, N. Desai, P. Ilten, S. Mrenna, S. Prestel, C. O. Rasmussen, and P. Z. Skands, "An introduction to PYTHIA 8.2," *Comput. Phys. Commun.* **191** (2015) 159–177, `arXiv:1410.3012 [hep-ph]`.

[93] B. Andersson, G. Gustafson, G. Ingelman, and T. Sjostrand, "Parton Fragmentation and String Dynamics," *Phys. Rept.* **97** (1983) 31–145.

[94] T. Sjostrand, "Jet Fragmentation of Nearby Partons," *Nucl. Phys. B* **248** (1984) 469–502.

[95] P. Skands, S. Carrazza, and J. Rojo, "Tuning PYTHIA 8.1: the Monash 2013 Tune," *Eur. Phys. J. C* **74** (2014) no. 8, 3024, `arXiv:1404.5630 [hep-ph]`.

[96] J. R. Christiansen and P. Z. Skands, "String Formation Beyond Leading Colour," *JHEP* **08** (2015) 003, `arXiv:1505.01681 [hep-ph]`.

[97] P. Kotko, L. Motyka, and A. Stasto, "Color Reconnection Effects in J/ψ Hadroproduction," `arXiv:2303.13128 [hep-ph]`.

[98] O. Mattelaer, "On the maximal use of Monte Carlo samples: re-weighting events at NLO accuracy," *Eur. Phys. J. C* **76** (2016) no. 12, 674, `arXiv:1607.00763 [hep-ph]`.

[99] C. Andreopoulos *et al.*, "The GENIE Neutrino Monte Carlo Generator," *Nucl. Instrum. Meth. A* **614** (2010) 87–104, `arXiv:0905.2517 [hep-ph]`.

[100] P. Nason, S. Dawson, and R. K. Ellis, "The Total Cross-Section for the Production of Heavy Quarks in Hadronic Collisions," *Nucl. Phys. B* **303** (1988) 607–633.

[101] A. H. Rosenfeld, "The particle data group: growth and operations-eighteen years of particle physics," *Ann. Rev. Nucl. Part. Sci.* **25** (1975) 555–598.

[102] A. Buckley, J. Butterworth, D. Grellscheid, H. Hoeth, L. Lonnblad, J. Monk, H. Schulz, and F. Siegert, "Rivet user manual," *Comput. Phys. Commun.* **184** (2013) 2803–2819, `arXiv:1003.0694 [hep-ph]`.

[103] E. Rodrigues, "The Scikit-HEP Project," *EPJ Web Conf.* **214** (2019) 06005, `arXiv:1905.00002 [physics.comp-ph]`.